Retrieval of the columnar aerosol phase function and single-scattering albedo from sky radiance over land: simulations

Haoyu Yang and Howard R. Gordon

We present a retrieval scheme that can be used to derive the aerosol phase function and single-scattering albedo from the sky radiance over land. The retrieval algorithm iteratively corrects the aerosol volume scattering function, the product of the single-scattering albedo and the phase function, based on the difference between the measured sky radiance and the radiance calculated by solving the radiative transfer equation. It is tested first under ideal conditions, i.e., the approximations made in the retrieval algorithm totally agree with actual conditions assumed in creating the pseudodata for sky radiance. It is then tested under more realistic conditions to assess its susceptibility to measurement errors and effects of conditions not recognized in the retrieval algorithm, e.g., surface horizontal inhomogeneity, departures of the surface from Lambertian, and aerosol horizontal inhomogeneity. These simulations show that, in most cases, this scheme can retrieve the aerosol single-scattering albedo with high accuracy (within 1%) and can therefore be used to identify strongly absorbing aerosols. It can also produce meaningful retrievals of most aerosol phase functions: less than 5% error at 865 nm and less than 10% at 443 nm in most cases. Typically, the error in the volume scattering function is small for scattering angles $\leq 90°$, then increases for larger angles. Disappointing results in both the single-scattering albedo and the scattering phase function occur at 443 nm, either when there are large calibration errors in the radiometer used to measure the sky radiance or when the land reflection properties are significantly inhomogeneous.

OCIS codes: 010.1110, 030.5620, 280.0280, 290.0290.

1. Introduction

Aerosols are currently of considerable interest because of their role in biogeochemical cycling and climate.[1–3] Thus several space-borne visible and near-infrared (NIR) remote sensing systems have been planned that are capable of delineating their global distribution: the moderate-resolution imaging spectroradiometer,[4] the multiangle imaging spectroradiometer,[5] the polarization and directionality of the Earth's reflectance,[6] etc. However, interpretation of the remotely sensed top-of-atmosphere (TOA) radiance contributed by the aerosol in terms of its physical–chemical, or even optical, properties requires the use of aerosol models.[7,8] These aerosol models can be physical and chemical, in which the size distribution and index of refraction of each aerosol component are specified (on the basis of direct measurements[9]), and the optical properties derived from Mie theory[10,11]; completely optical, in which the aerosol phase function and single-scattering albedo are specified spectrally; or a combination of the two. Similarly, aerosol models are also required for atmospheric correction to enable remote sensing systems to retrieve the spectral reflectance of the Earth's surface.[12,13]

An aerosol network (AERONET)[14] has been established for the purpose of obtaining the optical properties of aerosols under a wide variety of conditions. This network consists of robotic radiometers that measure the radiance of the direct Sun and the angular distribution of the sky radiance. Thus far, analysis of this data has focused on the inversion of the aerosol optical thickness and sky radiance in the solar aureole (single-scattering angle $\Theta < 30°$) with methods developed by Nakajima and co-workers[15,16] to study the aerosol size distribution.[17] The resulting size distribution is then used with Mie theory to derive the full aerosol phase function. One desirable

The authors are with the Department of Physics, University of Miami, Coral Gables, Florida 33124.

Received 10 March 1997; revised manuscript received 29 August 1997.

0003-6935/98/060978-20$10.00/0

advantage of this is that the columnar aerosol optical properties are obtained, quantities that would be difficult to obtain by direct sampling. Other advantages include the fact that the aureole radiance is nearly independent of the surface albedo,[16] and, because only a small portion of the sky is examined, the atmosphere only has to be horizontally homogeneous over only that portion. A disadvantage is that Mie theory is used in the inversion, and more important, in extending the phase function over the full angular range. Studies[18] of light scattering by randomly oriented spheroids show significant departures (~50%) in the phase function between spheroids and volume-equivalent spheres for $\Theta \gtrsim 30°$.

In earlier papers, Gordon, Wang, and co-workers showed how the sky radiance,[19,20] or a combination of the sky radiance and the TOA radiance,[21,22] over the oceans could be used to retrieve the columnar aerosol phase function and single-scattering albedo directly, without the necessity of Mie theory. Later, Zhang and Gordon[23,24] applied similar ideas to retrieve two elements of the scattering phase matrix from measurements of the sky radiance and its linear polarization. The basic Wang and Gordon[19] algorithm is an extension of the research of Wendisch and von Hoyningen-Huene.[25] Briefly, the sky radiance can be computed by solving the radiative transfer equation (RTE) with an initial input of an arbitrary aerosol volume scattering function (product of the phase function and single-scattering albedo). Recursive procedures are then applied to correct the trial volume scattering function based on the difference between the calculated and the measured sky radiance. The RTE is solved at each iteration, so the final solution contains all the effects of multiple scattering. This is an example of what McCormick[26] refers to as implicit methods in inverse transport theory. Simulations show that the algorithm can successfully retrieve the single-scattering albedo and aerosol phase function even when the aerosol optical thickness is as high as 2.[21]

The Wang and Gordon algorithm was designed originally to facilitate the retrieval of the aerosol single-scattering albedo and phase function over the ocean, and until now, has not been modified for operation over land. There are intrinsic differences between ocean surfaces and land surfaces. First, land surfaces are much brighter than ocean surfaces. They more strongly influence the sky radiance; therefore they are expected to have a negative impact on retrieval. Next, the bidirectional reflectance distribution functions (BRDF's) for land surfaces are much more complicated than those for ocean surfaces. The BRDF's for the ocean surface in the NIR can be described basically by a universal relationship, the only variable of which is the wind speed.[27–29] No such relationship exists for land surfaces. Finally, the land surface tends to be a much more horizontally heterogeneous reflector than the ocean surface.

In this paper we modify the Wang and Gordon algorithm for application over land for retrieving the aerosol single-scattering albedo and volume scattering function. First we illustrate the basic procedure of the retrieval algorithm. Next we provide simulation results assuming the measurements are made under ideal conditions and are error free. Finally, we assess the effects on the retrievals of measurement errors and various conditions that may exist in practice, yet are not taken into account in the retrieval algorithm, including surface horizontal inhomogeneity, aerosol horizontal and vertical inhomogeneity, and a non-Lambertian surface.

2. Basic Procedure of the Retrieval Algorithm

The total optical thickness of the atmosphere includes the optical thickness of Rayleigh scattering τ_r, the optical thickness of aerosol scattering τ_a, the optical thickness of the ozone layer τ_{Oz}, and the optical thickness of other absorbing gases τ_g. τ_r is stable, and given the surface pressure, can be computed at each wavelength.[30] τ_g, even though it is not so stable, is insignificant except in absorption bands. If one performs measurements between the absorption bands of absorbing gases, τ_g can generally be neglected.[31] Ozone absorption occurs throughout the visible and cannot be neglected. Also, τ_{Oz} is highly variable. However, it can be measured with spaceborne sensors, e.g., the total ozone mapping spectrometer,[32] or directly from the surface with spectral extinction.[33] Therefore it is possible to obtain the aerosol optical thickness by subtracting τ_r and τ_{Oz} from the measured total optical thickness. Thus we assume that τ_a can be obtained from measurements of solar extinction.

The basic procedure in the algorithm is as follows:

(1) measure the sky radiance and the aerosol optical thickness;

(2) estimate the surface albedo from direct measurements at the surface, supplemented by spaceborne observations if necessary;

(3) calculate the sky radiance by solving the RTE with an arbitrary aerosol volume scattering function, the measured aerosol optical thickness, and the land albedo;

(4) adjust the aerosol volume scattering function based on the difference between the measured sky radiance and the calculated sky radiance;

(5) interpolate and extrapolate the adjusted volume scattering function and use it to recalculate the sky radiance; and

(6) repeatedly apply steps (3), (4), and (5).

The volume scattering function V is defined as follows:

$$V(\hat{\xi}_0 \rightarrow \hat{\xi}) = \frac{\omega_0}{4\pi} P(\hat{\xi}_0 \rightarrow \hat{\xi}), \tag{1}$$

where ω_0 is the single-scattering albedo and P is the scattering phase function. (This definition differs from the ordinary definition of the volume scattering function[34] β, the differential scattering cross section per unit volume, by a factor of c, which is the extinc-

tion coefficient: $\beta = cV$.) The centerpieces of implementing the above algorithm are to (1) develop a computer code to solve the RTE for radiance given an aerosol volume scattering function, and (2) establish a relationship between the error in the volume scattering function $\Delta V_a(\Theta)$, and $\Delta L_t(\hat{\xi})$, the difference between the calculated radiance and the measured sky radiance.

To solve the RTE, we make the following assumptions and approximations. First we assume that the aerosol and Rayleigh scattering are confined between parallel planes. Also, because in reality approximately 80% of the aerosols are confined to a layer extending approximately 2 km above the ground or the ocean, and approximately 80–90% of the Rayleigh scattering is distributed above the aerosol layer,[35] we assume that the atmosphere is divided into two layers. The upper layer is exclusively Rayleigh scattering and the lower layer contains only aerosols. The above atmospheric model is known as the two-layer plane-parallel model. The ozone layer and other absorbing gases are neglected. The ozone layer can be treated conveniently as a fully absorptive layer above the TOA, and therefore can be incorporated easily into the retrieval algorithm. As for other absorbing gases, one can generally choose the wavelength windows between strong absorption bands of absorbing gases, where the effect of absorbing gases are not significant. We further assume that the land surface as well as the atmosphere is horizontally homogeneous and that the land surface is Lambertian. With the above approximations and assumptions, one can solve the RTE with the successive order method.[25] The details of implementing this are provided by van de Hulst.[36]

Now that we can solve the RTE, the next challenge is to find the relationship between ΔV_a and ΔL_t. It is sometimes desirable to distinguish between the radiance resulting from Rayleigh scattering and the radiance resulting from aerosol scattering. The total radiance can be divided into the following terms:

$$L_t = L_r \exp(-\tau_a/\mu) + L_a \exp(-\tau_r/\mu_0) + L_{ra}, \quad (2)$$

where L_r is the radiance contributed by Rayleigh scattering in the absence of aerosol scattering, L_a (Ref. 37) is the radiance contributed by aerosol scattering in the absence of Rayleigh scattering, and L_{ra} (Ref. 37) is the radiance contributed by the interaction between aerosol scattering and Rayleigh scattering. μ and μ_0 are, respectively, the cosines of the viewing zenith angle and the solar zenith angle.

Suppose the sky radiance is simulated with an aerosol volume scattering function different from the true one. The calculated sky radiance is naturally different from the measured sky radiance, i.e.,

$$\Delta L_t(\hat{\xi}_i) \equiv L_t^{(c)}(\hat{\xi}_i) - L_t^{(m)}(\hat{\xi}_i), \quad (3)$$

where $L_t^{(m)}$ is the measured sky radiance, $L_t^{(c)}$ is the calculated sky radiance, and $\hat{\xi}_i$ is the ith viewing direction. As none of $\Delta L_t(\hat{\xi}_i)$ result from pure Rayleigh scattering,

$$\Delta L_t(\hat{\xi}_i) = \Delta L_a(\hat{\xi}_i)\exp(-\tau_r/\mu_0) + \Delta L_{ra}(\hat{\xi}_i). \quad (4)$$

Our goal is to find $V(\Theta_i)$, where Θ_i is the scattering angle from the solar beam to the ith viewing direction, such that $\Delta L_t(\hat{\xi}_i) = 0$ for all i. This is effected with a modified Newton–Raphson algorithm.[38] When $V(\Theta_i) \rightarrow V(\Theta_i) + \Delta V(\Theta_i)$, $L_t^{(c)}[\hat{\xi}_i; V(\Theta)] \rightarrow L_t^{(c)}[\hat{\xi}_i; V(\Theta) + \Delta V(\Theta)]$. To first order in $\Delta V(\Theta_i)$,

$$L_t^{(c)}[\hat{\xi}_i; V(\Theta) + \Delta V(\Theta)] - L_t^{(m)}(\hat{\xi}_i) = L_t^{(c)}[\hat{\xi}_i; V(\Theta)] - L_t^{(m)}(\hat{\xi}_i) + \sum_j \frac{\delta L_t^{(c)}[\hat{\xi}_i; V(\Theta)]}{\delta V(\Theta_j)} \Delta V(\Theta_j). \quad (5)$$

Evaluation of the functional derivative $\delta L_t^{(c)}[\hat{\xi}_i; V(\Theta)]/\delta V(\Theta_j)$ is made by assuming that $L_{ra}(\hat{\xi})$ is negligible and that $\delta L_t^{(c)}[\hat{\xi}_i; V(\Theta)]/\delta V(\Theta_j)$ results mostly from single scattering. This is apparently a good approximation because the single-scattering contribution is proportional to $V(\Theta_j)$, whereas the multiple-scattering contributions and $L_{ra}(\hat{\xi})$ involve integrals of two or more volume scattering functions over a solid angle (see Subsection 4.E.1.2). Then note that the left-hand side of Eq. (5) is to be zero,

$$\Delta L_t(\hat{\xi}_i) = \frac{L_a(\hat{\xi}_i)\exp(-\tau_r/\mu_0)}{V(\Theta_i)} \Delta V(\Theta_i), \quad (6)$$

which is the desired relationship between $\Delta L_t(\hat{\xi}_i)$ and $\Delta V(\Theta_i)$. As approximations were made in the evaluation of the functional derivative, Eq. (6) is not precise. If it is used without modification in the iterative procedure illustrated at the beginning of this section, the calculated sky radiance often diverges instead of converging to the measured sky radiance. To solve this problem, we devised a self-adjusting constant C to ensure the convergence of the calculated radiance:

$$[V_a(\Theta_i)]_{\text{new}}^{(c)} = [V_a(\Theta_i)]_{\text{old}}^{(c)} + C\Delta[V_a(\Theta_i)]^{(c)}, \quad (7)$$

where $\Delta[V_a(\Theta_i)]^{(c)}$ is $\Delta V_a(\Theta_i)$ calculated in Eq. (6), $[V_a(\Theta_i)]_{\text{old}}^{(c)}$ is the volume scattering function used in the previous iteration, and $[V_a(\Theta_i)]_{\text{new}}^{(c)}$ is the new trial volume scattering function. The initial value of C is set to 1. In each iteration, the algorithm keeps track of the previous average value of $|\Delta L_t(\hat{\xi}_i)/[L_a^{(c)}(\hat{\xi}_i)\exp(-\tau_r/\mu_0)]|$. If it increases, which suggests that the $|V_a^{(c)}(\Theta_i)|$ is overcorrected, C is decreased by half. When there are relatively large errors in the measurements, C may become too small. In this case, C is reset to 1. In numerical analysis, C is often referred to as a relaxation parameter.[38]

The retrieval algorithm is almost complete up to this point. However, it is necessary to define criteria to terminate the iteration. The criteria we used in the retrieval algorithm are (1) the average absolute percentage difference between the measured sky radiance and the calculated radiance in all measurement directions is smaller than a certain threshold value (0.1%), and the maximum percentage differ-

ence is smaller than twice that value; or (2) the number of iterations exceeds a certain value (100). Once the iteration stops, the single-scattering albedo and phase function can be obtained by applying the following equations:

$$\omega_0 = \int_{4\pi} V_a(\Theta)\mathrm{d}\Omega, \tag{8}$$

$$P_a(\Theta) = 4\pi \frac{V_a(\Theta)}{\omega_0}. \tag{9}$$

Other than the fact that the lower boundary of the medium is a Lambertian reflector as opposed to a Fresnel reflector, there are few differences between the above-illustrated retrieval algorithm and the original Wang and Gordon algorithm for use over the ocean. The most significant difference is the assignment of C as a self-adjusting relaxation parameter. This reduces the number of iterations in each run.

3. Basic Simulation Results

A. Simulation of the Sky Radiance

To evaluate the performance of the retrieval algorithm, we used simulated measurements. However, we do take into consideration the practicality of these measurements so that they can be made in real situations. The radiance in the simulated measurements can be obtained by solving the RTE. A variety of aerosol models with different aerosol optical thicknesses have been used to generate the pseudodata for the sky radiance. The performance of the retrieval algorithm is evaluated by comparing the retrieved volume scattering function with the aerosol volume scattering function used in creating the pseudodata, henceforth referred to as the true aerosol volume scattering function.

The proposed measurements of sky radiance include almucantar measurements and principal plane measurements. In the almucantar measurements, one first aims the detector directly at the Sun ($\theta_v = \theta_0$, $\phi_v = 0$). While keeping the zenith angle of the detector fixed, one increases the azimuth angle ϕ_v of the detector by fixed increments until it reaches 180°. Subsequent to the almucantar measurements, in the principal plane measurements one keeps the azimuth angle of the detector at 180° and increases the zenith angle of the detector by fixed increments until it is almost horizontal.

In our simulations, the solar zenith angle is fixed to 60° in all cases. The increments in both the almucantar measurements and the principal plane measurements are set at 5°. The almucantar measurement at $\phi_v = 0$ is excluded, because it is impossible in actual measurements to separate the scattered light from the direct Sun light when the detector points at the Sun. Two additional measurements are taken in the almucantar measurements at $\phi_v = 3°$ and $\phi_v = 7°$ to obtain more information on the aerosol volume scattering function at small angles, because most aerosol phase functions are strongly forward peaked. At $\phi_v = 3°$, ($\theta_v = 60°$) the scattering angle from the Sun to the detector is 2.59°. This is the smallest angle at which a volume scattering function can be obtained from the measurements. The volume scattering function at scattering angles smaller than 2.59° has to be obtained through extrapolation. Note that currently, the smallest scattering angle from the Sun to the detector at which the radiance can be measured accurately is approximately 2°.[15] Therefore it is practical to measure the sky radiance at $\Theta = 2.59°$; however, for the radiometers used in AERONET, the smallest scattering angle is 3°.[14] In the principal plane measurements, the largest zenith angle of the detector is set at 85°. Therefore, in the sky radiance measurements, the largest single-scattering angle achievable is $\Theta = \theta_0 + 85° = 145°$. At any scattering angle larger than 145°, the phase function has to be extrapolated. We extrapolate the phase function by assuming that it is the same beyond 145° as it is at 145°.

Throughout this section, it is assumed that no error is incurred in these measurements. In addition, it is assumed that these measurements are conducted under ideal conditions, i.e., the conditions under which the measured radiance is produced are identical to those in the retrieval algorithm. To be more specific, the two-layer plane-parallel atmosphere model and the horizontal homogeneity assumption of aerosols and land surfaces, along with the approximation of a Lambertian surface, all of which are used in the retrieval algorithm, are adopted in generating measured radiance. The same values of the land albedos and aerosol optical thicknesses were used in both the retrieval algorithm and the sky radiance simulation program.

B. Retrieval Results

Rayleigh scattering can have a significant influence on the total radiance, especially when the scattering angle from the solar beam to the detector is large. To assess possible effects of Rayleigh scattering on the retrieval results, we applied the retrieval algorithm at wavelengths of 865 and 443 nm. The optical thickness for Rayleigh scattering is 0.01554 at 865 nm and 0.2361 at 443 nm at standard surface pressure.[30] These values are used throughout this paper.

We use the algorithm described here to understand the properties of aerosols in coastal areas, therefore, we concentrate on aerosol models most likely to represent aerosols near the coast. For this purpose, we use the Gordon and Wang[12] coastal aerosol model at 80% relative humidity (RH), C80, in most computations. However, because we also want to examine the performance of the algorithm under more general conditions, we also carried out tests using several aerosol models described by Shettle and Fenn.[10] These include their urban models at RH = 0% (U00), RH = 99% (U99), and their tropospheric model at RH = 80% (T80). These aerosols provide a range of shapes for the volume scattering function and a range

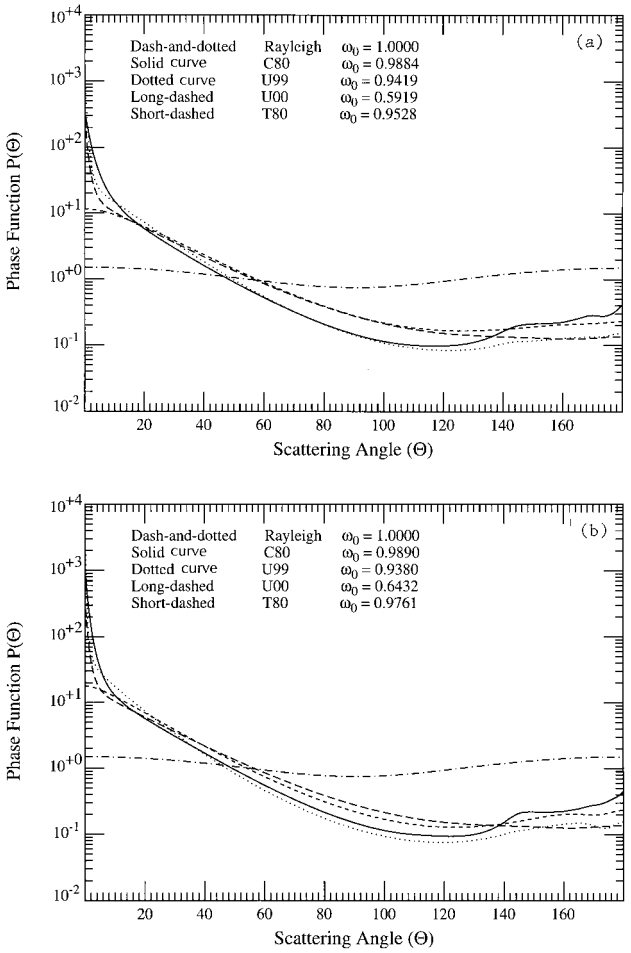

Fig. 1. Phase functions and single-scattering albedos for the aerosol models used in this study: (a) λ = 865 nm and (b) λ = 443 nm.

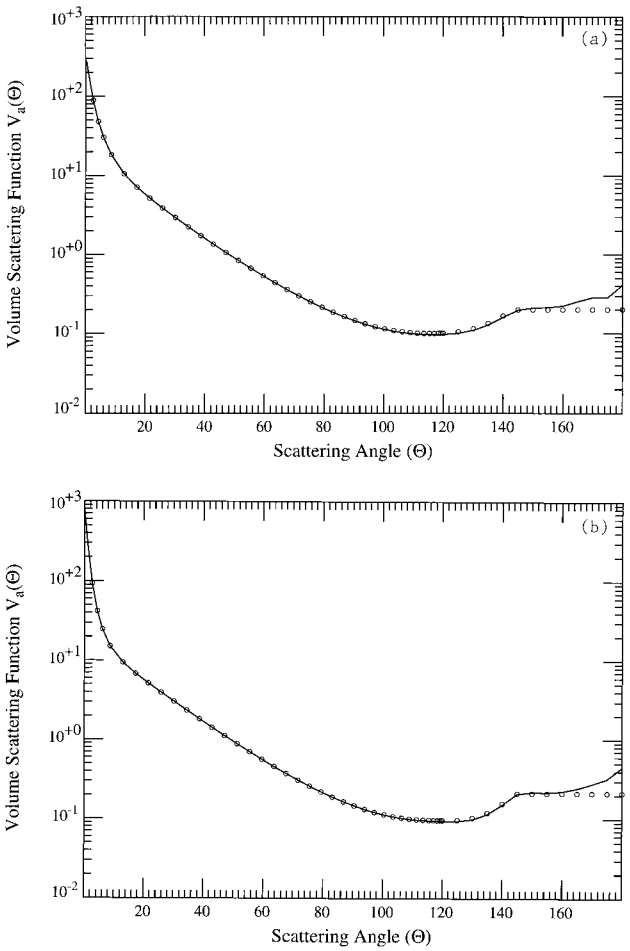

Fig. 2. Comparison between the true (curves) and retrieved (open circles) $V_\alpha(\Theta)$ for the C80 aerosol model: (a) λ = 865 nm and (b) λ = 443 nm.

of values for the single-scattering albedo. The phase functions and values of the single-scattering albedos for these models at 865 and 443 nm are provided in Fig. 1. In this figure, the phase functions for Rayleigh scattering are represented by dashed and dotted curves, and the phase functions of C80, U99, U00, and T80 are represented by solid curves, dotted curves, long dashed curves, and short dashed curves, respectively.

The coastal aerosol model is expected to be representative of aerosols found in coastal areas. They have a component of relatively large sea salt particles in addition to the aerosol in the T80 model. Beside the sharp peak at small scattering angles, the phase functions for C80 also have a significant structure for $\Theta > 120°$. The tropospheric aerosol model is used for aerosols in the troposphere, which are the small-particle component of aerosols expected to be found in rural areas free of pollution. Compared with the C80 aerosol at both wavelengths, the phase functions for T80 are less forwardly peaked. Urban aerosols are normally found in heavily polluted urban areas. They are composed of both large and small particles. The phase functions for U99 are extremely sharp at near-zero scattering angles. The phase functions for U00 are milder in forward directions, but the aerosol is highly absorbing. The single-scattering albedo for U00 at 865 and 443 nm are 0.5919 and 0.6432, respectively. In backward directions, the phase functions for both U99 and U00 are much smoother compared with those for C80. Thus our models span a considerable range of shapes for $P(\Theta)$ and values of ω_0.

Figure 2 shows the comparison of the true volume scattering functions and the retrieved volume scattering functions for the C80 aerosol at 865 and 443 nm. The true volume scattering functions are represented by solid curves and the retrieved volume scattering functions are represented by open circles. The land albedo is set to 1.0 at 865 nm and 0.5 at 443 nm because most vegetated surfaces have a smaller albedo in the blue than in the NIR. Note that these albedos are also larger than would be found in nature.[39,40] We use these larger surface albedos to make the retrieval more difficult for the algorithm. The optical thickness of the aerosol is set to 0.2 in Figs. 2(a) and 2(b) for comparison purposes. (In reality, the optical thickness of the aerosol layer would be larger at 443 nm than at 865 nm.) In both figures, the retrieved volume scattering functions are

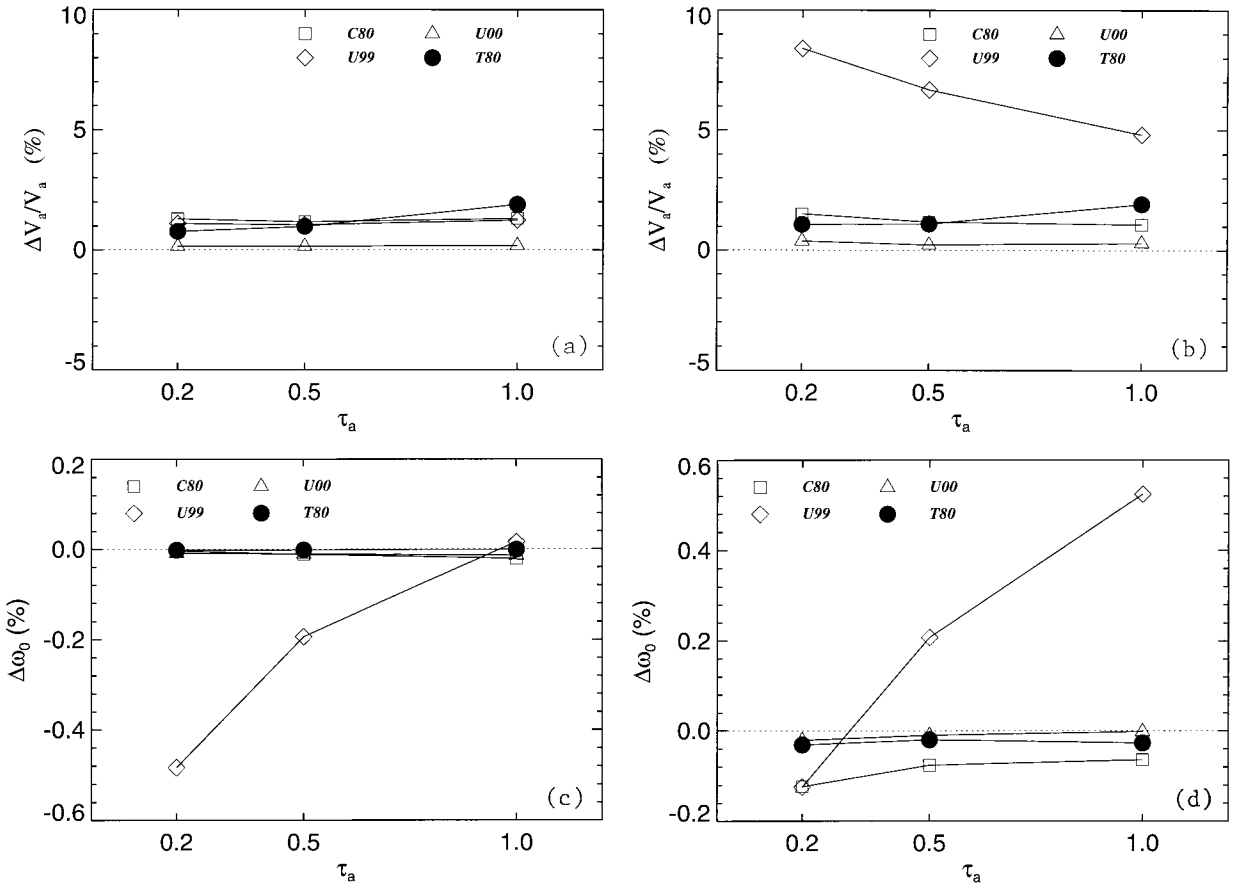

Fig. 3. Retrieval errors as a function of τ_a under ideal conditions: (a) and (b) error in the aerosol volume scattering function at $\lambda = 865$ nm and $\lambda = 443$ nm, respectively; (c) and (d) error in the aerosol single-scattering albedo at $\lambda = 865$ nm and $\lambda = 443$ nm, respectively.

almost perfect at small angles. They start to deviate from the true volume scattering functions at large angles because of the inability to obtain data beyond $\Theta = 145°$.

We define the error in the aerosol single-scattering albedo $\Delta\omega_0$ as

$$\Delta\omega_0 = \frac{\omega_0^{(c)} - \omega_0^{(t)}}{\omega_0^{(t)}}, \tag{10}$$

where $\omega_0^{(c)}$ is the retrieved aerosol single-scattering albedo and $\omega_0^{(t)}$ is the true single-scattering albedo, and we define the average error in the volume scattering function $\Delta V_a/V_a$ as

$$\Delta V_a/V_a = \frac{1}{N}\sum_{i=1}^{N}\left|\frac{[V_a(\Theta_i)]^{(c)} - [V_a(\Theta_i)]^{(t)}}{[V_a(\Theta_i)]^{(t)}}\right|, \tag{11}$$

where N is the number of measurements of L_t in a data set. Note that the definition of $\Delta V_a/V_a$ does not include the error in the volume scattering function for scattering angles smaller than 2.59° or larger than 145°. For the inversions shown in Fig. 3, $\Delta\omega_0 = -0.004\%$, $\Delta V_a/V_a = 1.29\%$ at 865 nm, $\Delta\omega_0 = -0.123\%$, and $\Delta V_a/V_a = 1.54\%$ at 443 nm.

Figure 3 shows the retrieval errors for C80, T80, U99, and U00 at 865 and 443 nm as a function of τ_a. The land albedo is set to 1.0 at 865 nm and 0.5 at 443 nm. The overall retrieval results are excellent. For most aerosols, retrieval errors in the volume scattering functions are within 2%, and retrieval errors in the single-scattering albedo are within 0.1%. These small errors are particularly impressive considering the large values assumed for the surface albedo. It is worth mentioning that the retrieval results for U00, the strongly absorbing aerosol, are extremely good, which suggests that the retrieval algorithm can be used to identify absorbing aerosols. This is in agreement with the conclusions of King and Herman.[41] The retrieval results for U99 are somewhat disappointing. The errors in the single-scattering albedo and especially the volume scattering function are significantly larger than for the other aerosol models. The explanation of this is provided at the end of this section.

In Fig. 3(c) it can be seen that the error in ω_0 could reach as much as -0.5%. Although this seems small, if ω_0 is near unity this can result in a significant error in the heating rate of the atmosphere. The heating rate is proportional to the co-albedo ω_c defined to be $1 - \omega_0$. For weak absorption, $\omega_c \approx 0$, so a small percent error in ω_0 can yield a much larger percent error in ω_c. For example, for U99, $\omega_0 = 0.938$, so $\omega_c = 0.062$, and a 0.5% error in ω_0 becomes an 8% error in ω_c and in the aerosol heating rate. All

methods for estimating absorption from sky radiance data are subject to this problem. However, note that in the case of strong absorption, e.g., U00, ω_0 is not near unity, so the relative error in the heating rate and ω_0 are similar.

Multiple scattering increases as the aerosol optical thickness increases. The more that multiple scattering contributes to the total radiance, the more diffuse the total radiance becomes. In general, the more diffuse the radiance, the harder it is to retrieve the volume scattering function. However, this assertion is not manifest in the figures so far shown. The aerosol optical thickness does not, in the region of interest, have a significant negative effect on the retrieval results. This may be due to the special design of the retrieval algorithm. Recall that iteration terminates after the average error in the volume scattering function is smaller than a certain value. [The error in the volume scattering function is approximated by $\Delta L_t/L_a \exp(-\tau_r/\mu_0)$ in Eq. (6).] Therefore the accuracy of the retrieved volume scattering function is not the ultimate accuracy that the retrieval algorithm could achieve, but rather is the accuracy specified by the user. Had the retrieval algorithm been designed to obtain the maximum accuracy, the accuracy at a lower optical thickness could have been higher than that at a higher optical thickness. For example, we observed that for a lower optical thickness, fewer iterations were required for the retrieval algorithm to obtain the aerosol volume scattering function with the same accuracy. Even though our tests do not show the ultimate accuracy that is achievable at different aerosol optical thicknesses, they do show that the retrieval algorithm is successful even when the aerosol optical thickness is as high as unity.

The presence of a thick Rayleigh scattering layer has a significant influence on the total radiance in directions where the scattering angles from the solar beam to the detector are large. However, inasmuch as it is shown in the retrieval results, Rayleigh scattering, despite having significant influence on the sky radiance, does not have much impact on the retrieval accuracy of either the single-scattering albedo or the volume scattering function. Even though the retrieval results for U99 are much worse at 443 nm than at 865 nm, the poorer performance at 443 nm is believed to be caused by the extrapolation error resulting from a much sharper phase function at 443 nm, rather than from the Rayleigh scattering itself. This outcome is surprising but understandable. Because Rayleigh scattering can be calculated accurately, it does not contribute to the difference between the measured radiance and the calculated radiance, as long as the measured radiance is error free.

In most of our simulations, relatively large errors are found in the volume scattering function near $\Theta = 0°$. Especially for U99, the errors in the volume scattering function at 0° are approximately −50% at 865 nm and approximately −93% at 443 nm, which means that the real volume scattering function at 0° is more than 12 times larger than the retrieved function. The results are not surprising. Close observation (Fig. 1) shows that the phase functions for U99 take an abrupt upward turn at around 2° and increase dramatically as the scattering angle decreases. Therefore the extrapolation of the phase functions at near-zero scattering angles is not likely to yield accurate results. However, notwithstanding the large errors at near-zero angles made in extrapolation, the retrieval results for U99 at 865 nm are surprisingly good. Errors in the volume scattering function are slightly over 1% at each optical thickness. The error in the single-scattering albedo is −0.5% for $\tau_a = 0.2$, slightly larger than for other models, but as τ_a increases, the error becomes smaller. The retrieval results at 443 nm are significantly poorer. The average errors in the volume scattering function are 8.40%, 6.68%, and 4.81% for $\tau_a = 0.2$, 0.5, and 1.0, respectively. They are significantly larger than for other models. The larger errors in the volume scattering function are due to inaccurate extrapolation at near-zero angles.

To understand the effect of extrapolation, one has to consider multiple scattering. In this section, we consider only multiple scattering as high as the second order. Higher-order scatterings and the surface contribution are neglected. We believe the omission of these processes does not affect our qualitative assertions. In this case, the total radiance L_t can be expressed as

$$L_t = L_{10} + L_{20}, \tag{12}$$

where L_{10} and L_{20} are the first- and second-order scattering (without the surface contributions), respectively. Suppose the aerosol optical thickness is low. If Rayleigh scattering is neglected, the downwelling single-scattering radiance at any aerosol optical thickness τ can be written as

$$L_{10}^{(d)}(\hat{\xi}') = F_0 \frac{\tau}{|\hat{\xi}' \cdot \hat{n}|} V_a(\hat{\xi}_0 \rightarrow \hat{\xi}'). \tag{13}$$

The upwelling single-scattering radiance can be written as

$$L_{10}^{(u)}(\hat{\xi}') = F_0 \frac{\tau_a - \tau}{|\hat{\xi}' \cdot \hat{n}|} V_a(\hat{\xi}_0 \rightarrow \hat{\xi}'), \tag{14}$$

where τ is defined such that at the TOA, $\tau = 0$ and $\tau = \tau_a$ at the surface.

One can obtain the second-order scattering by applying the single-scattering formula twice and integrating it over τ and over all solid angles. Neglecting higher orders of τ_a, one obtains

$$L_{20}(\hat{\xi}) = F_0 \frac{{\tau_a}^2}{2} \int_{4\pi} \frac{V_a(\hat{\xi}_0 \rightarrow \hat{\xi}') V_a(\hat{\xi}' \rightarrow \hat{\xi})}{|\hat{\xi}' \cdot \hat{n}||\hat{\xi} \cdot \hat{n}|} \, d\Omega(\hat{\xi}'). \tag{15}$$

Note that the integral does not converge, because the formula used for single scattering without a surface contribution is an approximate formula in which attenuation is neglected. Had the accurate single-

scattering formula been used, the integral would converge, e.g., see Ref. 16.

Suppose the retrieved volume scattering function is exact except at near-zero angles. Then an approximate formula for the extrapolation errors at near-zero solid angles with a delta function would be, i.e.,

$$V_a'(\hat{\xi} \rightarrow \hat{\xi}') = V_a(\Theta) - k\delta(\hat{\xi} - \hat{\xi}'), \tag{16}$$

where $V_a(\Theta)$ is the real volume scattering function and k is a positive constant. Note that k is simply the error in the single-scattering albedo when V_a' is taken to be the volume scattering function. It is easy to prove that, if Eq. (16) is used, the radiance is exact for single scattering. We obtained the error in the second-order scattering by combining Eqs. (15) and (16):

$$\Delta L_t(\hat{\xi}) = kF_0\tau_a{}^2 \frac{V_a(\hat{\xi}_0 \rightarrow \hat{\xi})}{|\hat{\xi}_0 \cdot \hat{n}||\hat{\xi} \cdot \hat{n}|}. \tag{17}$$

Comparing it with the single-scattering formula L_{s0}, Eq. (17) can be expressed as

$$\Delta L_t(\hat{\xi}) = k \frac{\tau_a L_{10}(\hat{\xi})}{|\hat{\xi}_0 \cdot \hat{n}|}. \tag{18}$$

Equation (18) reveals that the error in the radiance in any given direction is proportional to the product of the error in the single-scattering albedo (k) and the single-scattering radiance. If Rayleigh scattering is included, one can prove that Eq. (18) is still valid except that Rayleigh scattering has to be included in the single-scattering formula:

$$\Delta L_t(\hat{\xi}) = \frac{k\tau_a}{|\hat{\xi}_0 \cdot \hat{n}|}[L_{a10}(\hat{\xi}) + L_{r10}(\hat{\xi})], \tag{19}$$

where L_{10} has been expressed as a combination of Rayleigh scattering and aerosol scattering. Recall that the relative error in the volume scattering function was approximated by

$$\frac{\Delta V_a(\Theta)}{V_a(\Theta)} = \frac{\Delta L_t}{L_a \exp(-\tau_r/\hat{\xi}_0 \cdot \hat{n})}, \tag{20}$$

where L_a is the radiance in the absence of Rayleigh scattering. Substituting ΔL_t in Eq. (19) into Eq. (20), we obtain

$$\frac{\Delta V_a(\Theta)}{V_a(\Theta)} = k \frac{\tau_a}{\mu_0}\left[\frac{L_{a10} + L_{r10}}{L_a \exp(-\tau_r/\mu_0)}\right], \tag{21}$$

where μ_0 is the cosine of the solar zenith angle. In the absence of Rayleigh scattering, it is obvious that L_{a10}/L_a is always smaller than 1. Therefore the maximum relative error in the volume scattering function is limited roughly to $k\tau_a/\mu_0$. This explains why the error in the retrieved volume scattering function of urban aerosol at 865 nm is not influenced by the extrapolation error at near-zero angles. However, if the optical thickness of Rayleigh scattering is relatively large, L_{r10} can be much larger than L_a at larger scattering angles. In this case, although the small-angle scattering is not influenced by Rayleigh scattering because aerosol scattering is much more significant than Rayleigh scattering, errors at large scattering angles are magnified by Rayleigh scattering.

Examining Eq. (21) closely, we find that on the right-hand side, the dominant term in the numerator is L_{r10} at large scattering angles. It is independent of τ_a. On the other hand, as τ_a increases beyond the single-scattering limit, $L_a \sim a\tau_a + b\tau_a{}^2 + \cdots$, so when $L_{r10} \gg L_{a10}$,

$$\frac{\Delta V_a(\Theta)}{V_a(\Theta)} \propto \frac{1}{a + b\tau_a + \cdots}, \tag{22}$$

where a and b are constants. This explains the result that, when the aerosol optical thickness increases, the overall error in the volume scattering function becomes smaller.

4. Effects of Approximations and Measurement Errors

In Section 3 we evaluated the performance of the retrieval algorithm based on the assumption that measurements are taken under ideal conditions and are error free. However, in reality, the measurements contain errors, and the conditions assumed in the retrieval algorithm to calculate the sky radiance, e.g., the surface, are not usually Lambertian. The effects of measurement error and approximations can be quite significant. Therefore an understanding of these effects is necessary.

A. Effect of a Non-Lambertian Surface

In the retrieval algorithm, we assumed the land surface to be Lambertian, i.e., the surface reflectance is independent of the directions of the incident light and reflected light. In reality, the reflectance varies not only with the direction of the reflected light, but also with the direction of the incident light. Sometimes it may not even be symmetric about the principal plane,[42] the plane determined by the incident light and the direction normal to the surface. Accordingly, the Lambertian surface approximation used in the retrieval algorithm might cause significant error when applied to non-Lambertian surfaces.

The surface reflectance can be represented by the BRDF $R(\hat{\xi}_0 \rightarrow \hat{\xi})$, where $\hat{\xi}_0$ and $\hat{\xi}$ are the directions of the incident light and reflected light, respectively. The definition of R is as follows. If a beam of parallel light, with irradiance $E_0(\hat{\xi}_0)$ on a surface normal to the beam, is incident on a flat surface in a direction $\hat{\xi}_0$ and the radiance of the reflected beam in the viewing direction $\hat{\xi}$ is $L_{\text{ref}}(\hat{\xi})$, then the BRDF of the surface is

$$R(\hat{\xi}_0 \rightarrow \hat{\xi}) = \frac{\pi L_{\text{ref}}(\hat{\xi})}{E_0(\hat{\xi}_0)|\hat{\xi}_0 \cdot \hat{n}|}, \tag{23}$$

where $\hat{n}$ is the surface normal. For a Lambertian surface, the BRDF reduces to a simple form:

$$R(\hat{\xi}_0 \rightarrow \hat{\xi}) = \omega_l, \tag{24}$$

where ω_l is the surface albedo. The BRDF for geophysical surfaces is difficult to measure, as both $\hat{\xi}_0$ and $\hat{\xi}$ must be varied. Most observations of the directional reflection properties of such surfaces involve measurement of the reflectance factor $R_L(\hat{\xi}, \hat{\xi}_0)$ defined by

$$R_L(\hat{\xi}, \hat{\xi}_0) \equiv \frac{\pi L_{\text{ref}}}{E_{\text{total}}(\hat{\xi}_0)},$$

where $E_{\text{total}}(\hat{\xi}_0)$ is the total irradiance (Sun plus sky) falling on the surface (as usual, $\hat{\xi}_0$ is the direction of propagation of the solar beam). As both L_{ref} and $E_{\text{total}}(\hat{\xi}_0)$ contain the influence of the sky irradiance, it is clear that $R(\hat{\xi}_0 \rightarrow \hat{\xi})$ cannot be derived from $R_L(\hat{\xi}, \hat{\xi}_0)$ unless the sky contribution to E_{total} is much less than the Sun's contribution. This is a good approximation in the red and NIR portion of the spectrum if the measurements are made on relatively clear days (low aerosol concentration). We assume here that $R_L(\hat{\xi}, \hat{\xi}_0) = R(\hat{\xi}_0 \rightarrow \hat{\xi})$. Kimes *et al*. have measured $R_L(\hat{\xi}, \hat{\xi}_0)$ for several geophysical surfaces.[43] For our research, we examined the stepped grass and irrigated wheat surfaces. Kimes *et al*'s measurements were performed in two wavelength bands, the 580–680-nm band and the 710–1100-nm band, at three different solar zenith angles, 27°, 35°, and 63° for the stepped grass surface and 28°, 42°, and 59° for the irrigated wheat surface. At each solar zenith angle, measurements were taken at six viewing (reflected) zenith angles from 0° to 75° at intervals of 15° and for each zenith angle at five viewing azimuth angles from 0° to 180° at intervals of 45°.

These measurements confirm that the BRDF depends not only on the viewing direction but also on the solar direction. Furthermore, if we calculate the albedo by integrating the extrapolated and interpolated BRDF, we obtain

$$\omega_l(\hat{\xi}_0) = \frac{1}{\pi} \int_{\hat{\xi} \cdot \hat{n} > 0} R(\hat{\xi}_0 \rightarrow \hat{\xi}) |\hat{\xi} \cdot \hat{n}| \, \mathrm{d}\Omega(\hat{\xi}), \qquad (25)$$

where $\hat{n}$ is an unit vector normal to the surface pointing upward and the resulting albedos are different at different Sun angles. For the stepped grass surface at the solar zenith angles of 27°, 35°, and 63°, the albedos are 0.2334, 0.2254, and 0.1948, respectively, in the 580–680-nm band and 0.3113, 0.3253, and 0.2917 in the 730–1100-nm band. The albedos for the irrigated wheat surface at the solar zenith angles of 28°, 42°, and 59° are, respectively, 0.0467, 0.0522, and 0.0819 in the 580–680-nm band and 0.4107, 0.4785, and 0.5857 in the 730–1100-nm band.

To test the performance of the retrieval algorithm, we applied it to both the stepped grass surface and the irrigated wheat surface. To calculate the sky radiance, we have to know the value of the BRDF for all incident and reflected directions. Assuming $R_L = R$ at the solar zenith angles at which the measurements were taken, the BRDF for any viewing directions other than those measured can be either interpolated or extrapolated. However, interpolation and extrapolation of the BRDF with respect to the solar zenith angle is not likely to produce any meaningful results as we have only three solar zenith angles available. Therefore we assumed that the BRDF is independent of the zenith angle of the incident direction, even though the data clearly indicate otherwise. Thus we assume that $R_L(\hat{\xi}, \hat{\xi}_0) = R(\hat{\xi}_0 \rightarrow \hat{\xi})$ is independent of the zenith (but not the azimuth) angle of $\hat{\xi}_0$.

Figures 4(a) and 4(b) display the BRDF's, $R(\hat{\xi}_0 \rightarrow \hat{\xi})$, for the stepped grass surface in the 580–680-nm band and 730–1100-nm band, respectively, for a solar zenith angle of 63°. Figures 4(c) and 4(d) display the BRDF's for the irrigated wheat surface for a solar zenith angle of 59° in the 580–680-nm band and the 730–1100-nm band, respectively. The θ axis is the viewing zenith angle and the ϕ axis is the viewing azimuth angle. The vertical axis is the BRDF. The viewing angles are defined such that, when the reflected light travels in the direction opposite to the solar beam, the viewing zenith angle is the same as the solar zenith angle and the viewing azimuth angle is 180°. (The solar azimuth angle, ϕ_0 is 0 by definition.) Although measured for a specific solar zenith angle, these BRDF surfaces are taken to represent the BRDF for any zenith angle of an incident photon. In this case, ϕ in Figs. 4(a)–4(d) is the difference in azimuth between the incident and reflected directions.

These graphs share the feature that the BRDF increases as the viewing zenith angle and azimuth angle increase. In other words, the BRDF's are larger in directions close to the direction opposite to the solar beam. This is true for most natural surfaces.[44] However, the BRDF's for the stepped grass surface show much less total variation than for the irrigated wheat surface.

In the calculation of the sky radiance pseudodata, the non-Lambertian BRDF replaces the Lambertian surface. The solar zenith angle is set to 60° as usual. We choose the BRDF's measured at 63° and 59° to be the BRDF's for the stepped grass surface [Figs. 4(a) and 4(b)] and the irrigated wheat surface [Figs. 4(c) and 4(d)], respectively. The sky radiance is calculated at two wavelengths, 443 and 865 nm. Because we do not have information on the BRDF's at these wavelengths, the BRDF's in the 580–680-nm band and the 710–1100-nm band were used at 443 and 865 nm, respectively. The retrieval algorithm assumes a Lambertian surface and used the true values of the surface albedo that we obtained by integrating the BRDF. Figure 5 shows the retrieval results with the C80 aerosol model.

The results for the stepped grass surface are fairly good. At 865 nm, the largest error in the single-scattering albedo is less than 0.4%, and the largest average error in the volume scattering function is less than 5%. The results for the irrigated wheat surface are significantly poorer at 865 nm. The largest error in the single-scattering albedo is more than 2%, and the largest average error in the volume scattering function is more than 12.0%. The lower errors at

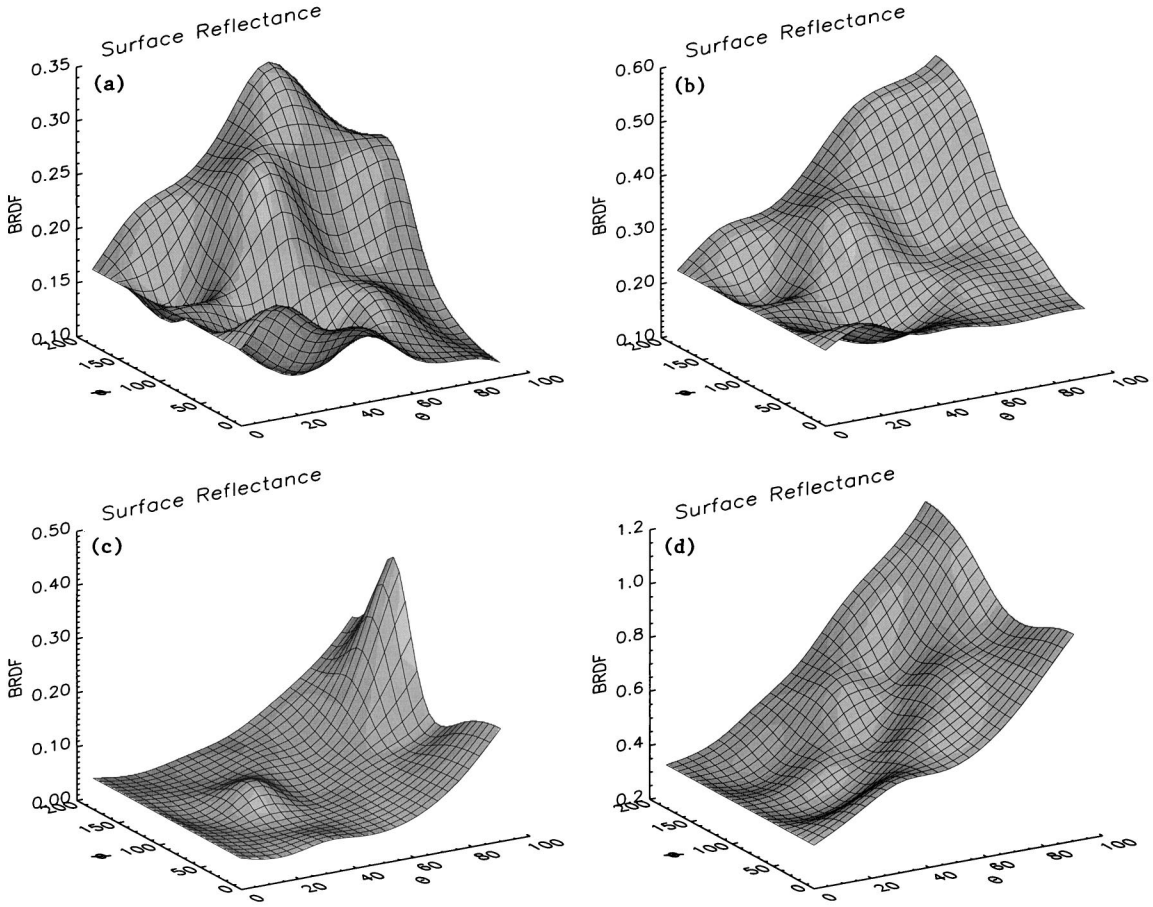

Fig. 4. BRDF for two surfaces: (a) and (b) stepped grass surface in bands 580–680 and 730–1100 nm, respectively, at $\theta_0 = 63°$; (c) and (d) irrigated wheat surface in bands 580–680 and 730–1100 nm, respectively, at $\theta_0 = 59°$.

443 nm are due to the lower albedo compared with 865 nm; however, note that at 443 nm, the stepped grass has a higher albedo (0.19) than the irrigated wheat (0.08), but the overall accuracy of the stepped grass retrieval is better. Thus the shape of the BRDF can be seen to play a significant role in interfering with the accuracy of the inversion algorithm.

B. Effect of Horizontally Inhomogeneity in the Surface Albedo

In addition to the fact that land is usually not Lambertian, it is usually covered with different surfaces that have different albedos. In urban areas, the land is covered with highways, roads, buildings, houses, lawns, trees, etc. Even in rural areas, where the landscape is much simpler, the land is usually covered by a mixture of crops, grasses, and bare soils. In these cases, the land is not horizontally homogeneous. Table 1 lists the albedos of different types of surfaces obtained from the Kimes *et al*. measurements.[42,43,45] The albedos vary with the solar zenith angle, but to simplify the table, we list only the albedos for solar zenith angles near 60°.

To simulate the inhomogeneity in land surfaces, we created a simple model—the checkerboard model. In the checkerboard model, as the name suggests, the land is divided equally into square patches. Two types of surface are assigned randomly to each patch. To create the maximum contrast, we used the approximate albedos of the hardwood forest and the grass land surface at 443 nm ($\omega_l = 0.05$ and 0.35, respectively) and soil and irrigated wheat at 865 nm ($\omega_l = 0.20$ and 0.60, respectively). In this case, we created the pseudodata using a Monte Carlo code. In the retrieval algorithm we used the average albedo as the albedo of the homogeneous Lambertian surface. That is, $\omega_l = 0.20$ at 443 nm and $\omega_l = 0.40$ at 865 nm. The Lambertian surface approximation was used in the sky radiance pseudodata calculation as well as in the retrieval algorithm.

To assess the effect of the size of each individual patch on the retrieval, we vary the size from 0.1×0.1 km^2 to 1.0×1.0 km^2. For each size, we generate ten independent random patterns. Figure 6 demonstrates the standard deviation of the retrieved $\omega_0^{(i)}$, $\delta\omega_0$, and the average value of $|\Delta V_a/V_a|^{(i)}$, $\overline{\Delta V_a/V_a}$, for each size. The x axis is the length (in kilometers) of each individual square patch. $|\Delta V_a/V_a|$ and $\delta\omega_0$ are represented by squares and triangles, respectively, at both wavelengths. In our calculation we assume that aerosol and Rayleigh scattering are vertically homogeneous. The upper boundary of the aerosol

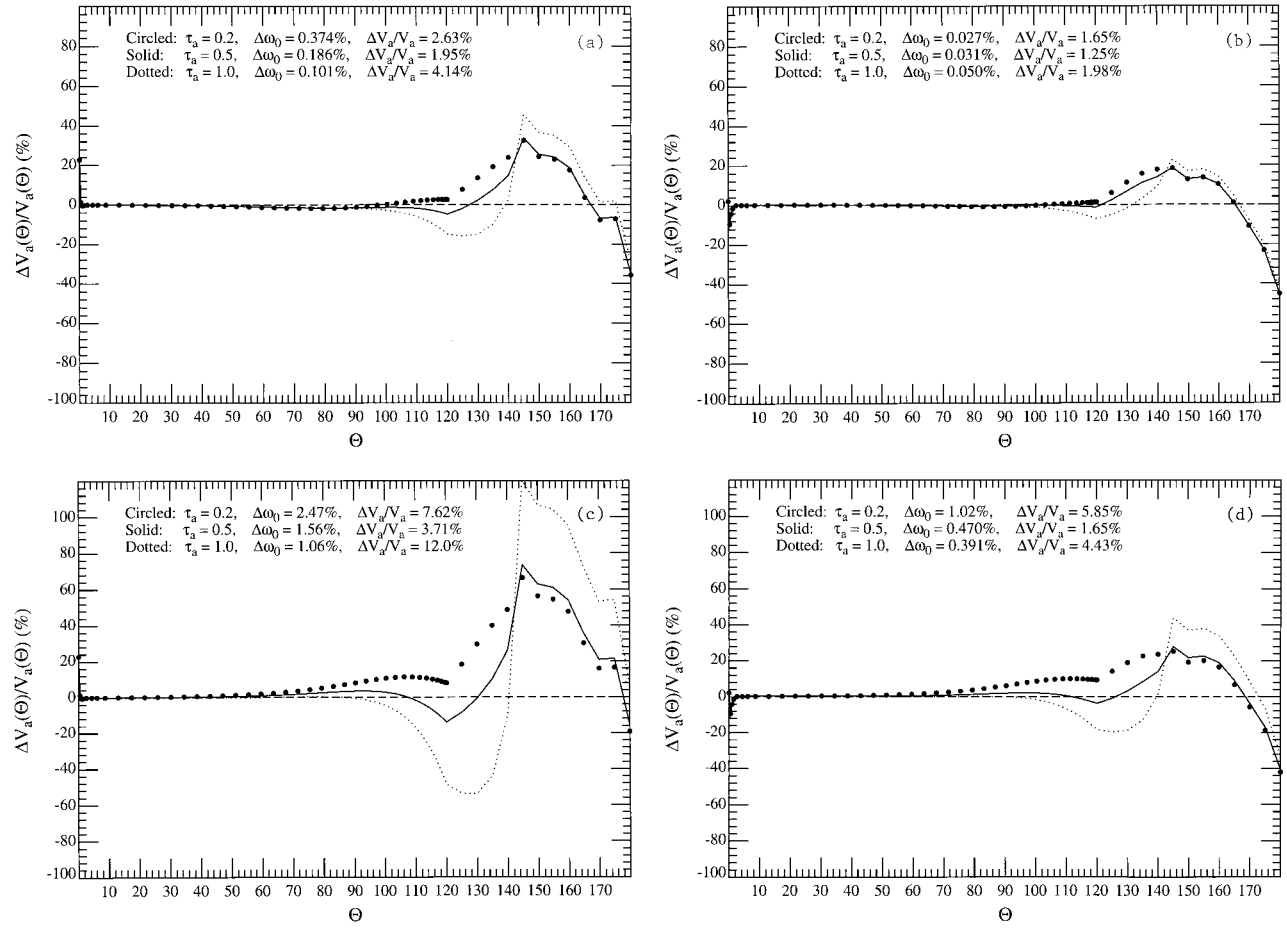

Fig. 5. Retrieval errors for non-Lambertian surfaces: (a) and (b) stepped grass surface at 865 and 443 nm, respectively; (c) and (d) irrigated wheat surface at 865 and 443 nm, respectively.

and the lower boundary of Rayleigh scattering are 1 km above the ground. The upper boundary of Rayleigh scattering is 7 km above the ground. $\tau_a = 0.20$ in all these cases. The results indicate that the size of the individual patch is crucial. The larger each individual patch, the larger the fluctuations in the retrieved volume scattering function and single-scattering albedo. When the land is divided into 0.1×0.1 km^2 patches, there is little effect resulting from the randomness of the land surface albedo. As the size of the patch increases, so does the fluctuation in the volume scattering function and the single-scattering albedo. Comparing the results at 443 nm with those at 865 nm, we found that Rayleigh scattering at 443 nm does not have a significant influence on retrieval.

These results can be understood through the fol-

Table 1. Albedos of Different types of Land Surface

Surface Type	580–680 nm	730–1100 nm
Soil	0.1885	0.2246
Grassland	0.3225	0.4307
Lawn grass	0.0841	0.5056
Orchard grass	0.0847	0.3424
Stepped grass	0.1948	0.2917
Soybeans	0.0544	0.5743
Corn	0.0693	0.3224
Irrigated wheat	0.0819	0.5857
Hard wheat	0.2310	0.4334
Pine forest	0.0655	0.2923
Hardwood forest	0.0467	0.3694

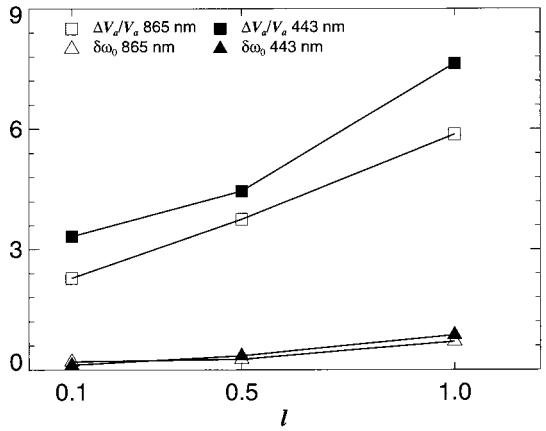

Fig. 6. $\overline{|\Delta V_a/V_a|}$ and $\delta\omega_0$ for the checkerboard model.

lowing analysis. In the single-scattering approach the surface contribution is represented by the following integral:

$$L_{1s}(\hat{\xi}) = F_0 \frac{|\hat{\xi}_0 \cdot \hat{n}|}{\pi} \int_{z_0}^{z_1} \int_{-\infty}^{+\infty} \int_{-\infty}^{+\infty} c_a \omega_l(x, y) \times \frac{V_a(\hat{\xi} \rightarrow \hat{\xi}')}{|\hat{\xi} \cdot \hat{n}|^2} \frac{|\hat{\xi}' \cdot \hat{n}|}{r^2(\hat{\xi}, z; x, y)} \mathrm{d}x\mathrm{d}y\mathrm{d}z, \quad (26)$$

where z_1 is the altitude of the upper boundary of the aerosol layer, z_0 ($z_0 = 0$) is the altitude of the lower boundary of the aerosol layer, and z is any altitude in between. c_a is the extinction coefficient of the aerosol; $\mathrm{d}x\mathrm{d}y$ is an infinitesimal area of the land surface; and ω_l, which is a function of x and y, is the surface albedo. $\hat{\xi}_0$ is the direction in which the solar beam propagates, $\hat{\xi}$ is the viewing direction, $r(\hat{\xi}, z; x, y)$ is the distance from the infinitesimal area to any position along the viewing direction $\hat{\xi}$, and ξ' is the unit vector along r.

The contribution to the radiance from a unit area is proportional to $|\hat{\xi}' \cdot \hat{n}|/r^2$. Therefore the closer the area is to the detector, the larger the influence it has on the radiance. Calculations show that more than 75% of the surface contribution from aerosol scattering is attributable to an area within a 3-km radius of the detector. When the length of each patch is 1.0 km, the fluctuation in the surface term is extremely large. In this case, the albedo of the actual patch on which the radiometer is located would be more appropriate to use in the algorithm than the mean albedo over a large area.

Equation (26) can be modified easily to include Rayleigh scattering. All that is needed is to add a similar integral that contains Rayleigh scattering. Because Rayleigh scattering molecules are distributed from 1 to 7 km above the ground, a wide area of surface contributes significantly to total sky radiance. The wide area contains a large number of patches of land. Consequently the fluctuation in the surface contribution from Rayleigh scattering is small. This explains why the retrieval results did not seem to be influenced by Rayleigh scattering, i.e., they were independent of wavelength. The message from these few tests with heterogeneous albedo appears clear: collect data over regions that are heterogeneous over small scales and use the average albedo in the inversions, or collect data over regions that are heterogeneous over large scales and use the local albedo.

C. Effect of Aerosol Horizontal Inhomogeneity

In the previous calculations, we assumed homogeneous aerosol density. In reality, the aerosol density varies both horizontally and vertically. As there is no straightforward way to assess the effect of aerosol horizontal inhomogeneity, we take an extreme approach. In the downwelling radiance calculation, we assume that all aerosols are confined in a square box. A detector is situated at the center of the bottom of the box. Aerosols are uniform within the box, but no aerosol exists outside the box. Because the aerosol inhomogeneity is so unrealistic, the results can be viewed only as an extreme example of the influence of horizontal inhomogeneity. In the retrieval program, the aerosol density is assumed to be homogeneous over the entire horizontal range. The value of the optical thickness within the box in the radiance calculation program is used in the retrieval algorithm. The C80 aerosol is used to generate the sky radiance in a Monte Carlo code. A Lambertian surface with a surface albedo of 1.00 at 865 nm and 0.5 at 443 nm was used in both the sky radiance calculation and the retrieval algorithm. The height of the box (h_{box}) is 1 km. The length of the square box (l_{box}) varies from 10 to 100 km. Figure 7 shows the retrieval results of the inhomogeneous aerosol at 865 and 443 nm, with box lengths of 10, 20, 50, and 100 km.

At both 865 and 443 nm, when the length of the box is 10 km, errors are relatively large compared with the results when the aerosol is homogeneous (Fig. 3). They become smaller as the length of homogeneity increases. When the length of homogeneity is 50 km, there is no significant error in either the single-scattering albedo or the volume scattering function resulting from aerosol inhomogeneity. A comparison of the two wavelengths shows that the results at 443 nm are poorer than those at 865 nm; however, the pattern of the error with increasing τ_a is the same at both wavelengths. The error in $V_a(\Theta)$ is principally at $\Theta \gtrsim 80°$ and is always negative to approximately $\Theta \sim 145°$. This error is caused by the detection of less sky radiance at large scattering angles for the smaller boxes. The magnification of the error from 865 to 443 nm. i.e., with increasing Rayleigh scattering, can be understood as follows. As the algorithm assumes that the aerosol layer is homogeneous, detection of less radiance will have the same effect as a negative error in the measured sky radiance. In Subsection 4.E below, we show that, all other things being equal, error in sky radiance at 443 nm has a more significant impact than error at 865 nm.

In conclusion, although these results apply only to the extreme aerosol distribution used in the simulations, they do suggest that when the range of horizontal homogeneity is 20 km, in other words, when the aerosol is homogeneous within 10 km of the detector, it is safe to treat the aerosol as horizontally homogeneous at 865 nm. In contrast, the prevalence of Rayleigh scattering at 443 nm requires the aerosol to be homogeneous over a larger distance, i.e., within 25 km of the detector.

D. Effects of Aerosol Vertical Structure

In reality, both the aerosol density and the Rayleigh scattering molecular density change with altitude. The vertical inhomogeneity of aerosol or Rayleigh scattering per se does not invalidate the two-layer model if the aerosol layer exclusively contains aerosol scattering and if the Rayleigh layer exclusively contains Rayleigh scattering. However, if there is a sig-

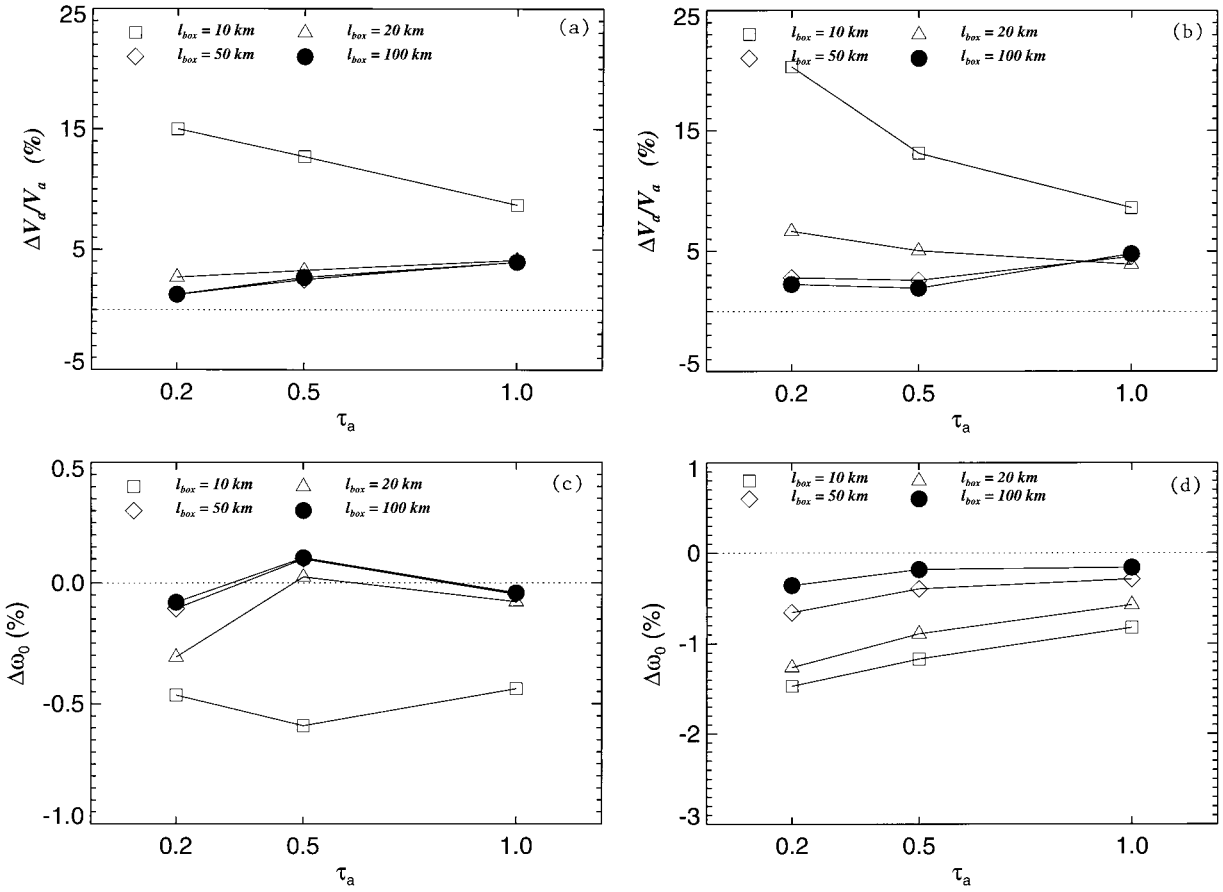

Fig. 7. Errors in V_a and ω_0: (a) and (b) error in V_a at 865 and 443 nm, respectively; (c) and (d) error in ω_0 at 865 and 443 nm, respectively.

nificant amount of Rayleigh scattering in the aerosol layer or vice versa, which is typically the case, it is necessary to reconsider the validity of the two-layer model.

Previous research by Zhang showed that, for most aerosols, the mixture of Rayleigh scattering and aerosol scattering does not have a significant influence on retrieval.[46] However, when the aerosol is strongly absorbing, significant errors can be incurred. Zhang's results are derived from retrieval over the ocean. To examine if this is also the case for retrieval over land, we used an extremely unrealistic model (the one-layer model) in which the aerosol and Rayleigh scattering are uniformly mixed.

We found that, for most weakly absorbing aerosols (C80, T80, and U99), under otherwise identical conditions, the sky radiance calculated by solving the RTE with the one-layer model at 443 and 865 nm does not differ significantly from that with the two-layer model. On the other hand, for absorbing aerosols (U00), the differences were significant at 865 nm and remarkably large at 443 nm. Therefore, in analyzing the effect of vertical inhomogeneity of aerosols and Rayleigh scattering molecules, we focused on strongly absorbing aerosols (U00).

Figures 8(a) and 8(b) show the retrieval results at 865 and 443 nm, respectively. The one-layer model is used to create the pseudodata for sky radiance and the two-layer model is used in retrieval. In both figures, the land is a Lambertian surface, $\omega_l = 1.0$ at 865 nm and $\omega_l = 0.5$ at 443 nm. At 865 nm, the retrieval results are fairly good. Errors in the single-scattering albedo and average errors in the volume scattering function for $\tau_a = 0.2$, 0.5, and 1.0 are roughly 1%. This is not difficult to understand because τ_r is very small at 865 nm. However, at 443 nm, errors in the single-scattering albedos for $\tau_a = 0.2$, 0.5, and 1.0 average 4.0% and errors in the volume scattering functions average nearly 15%. In both figures, we noticed that error in the volume scattering function increases dramatically from 120° to 145°. This is a region where the contribution of multiple scattering is particularly large.

This result can be understood by examining single scattering. For simplicity, we assume that the aerosol is totally absorptive. In the two-layer model, the single-scattering radiance $L_{10}{}^{2-\mathrm{lyr}}$ is given by

$$L_{10}{}^{2-\mathrm{lyr}}(\hat{\xi}) = F_0\mu_0 \exp(-\tau_a/\mu) \times \left[\frac{\exp(-\tau_r/\mu_0) - \exp(-\tau_r/\mu)}{\mu - \mu_0}\right] V_r(\Theta), \quad (27)$$

where μ_0 and μ are the cosines of solar zenith angle and viewing angle, respectively. In the one-layer

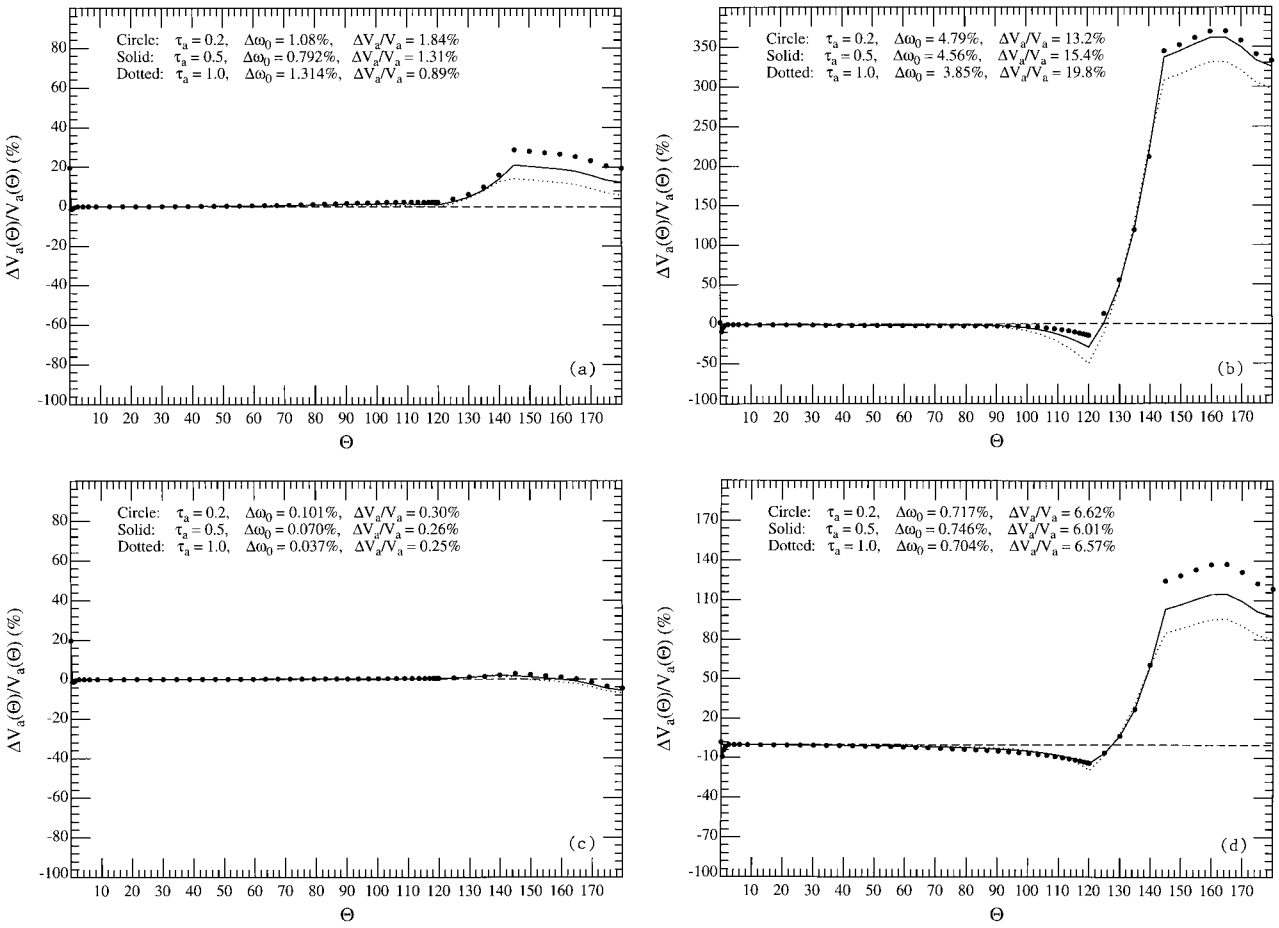

Fig. 8. Effect of vertical structure: (a) 865 nm for U00 with pseudodata created with the one-layer model; (b) 443 nm for U00 with pseudodata created with the one-layer model; (c) 865 nm for U00 with pseudodata created with the modified two-layer model; (d) 443 nm for U00 with pseudodata created with the modified two-layer model. In each case the original two-layer model is used for retrieval.

model, the equivalent volume scattering function is $\tau_r V_r/(\tau_a + \tau_r)$. Therefore, ${L_{10}}^{1-\mathrm{lyr}}$ is given by

$$
\begin{aligned}
{L_{10}}^{1-\mathrm{lyr}}(\hat{\xi}) = F_0\mu_0 & \\
\times & \left\{\frac{\exp[-(\tau_r+\tau_a)/\mu_0] - \exp[-(\tau_r+\tau_a)/\mu]}{\mu-\mu_0}\right\} \\
\times & \frac{\tau_r V_r(\Theta)}{\tau_a+\tau_r}. \qquad (28)
\end{aligned}
$$

If $\mu = \mu_0$, both Eq. (27) and Eq. (28) simplify to the same form:

$$
\begin{aligned}
{L_{10}}^{2-\mathrm{lyr}}(\hat{\xi}) &= {L_{10}}^{1-\mathrm{lyr}}(\hat{\xi}) \\
&= F_0\left\{\frac{\tau_r \exp[-(\tau_a+\tau_r)/\mu_0]}{\mu_0}\right\}V_r(\Theta). \qquad (29)
\end{aligned}
$$

Therefore in the single-scattering approach, the one-layer model does not have any influence on the radiance if $\mu = \mu_0$, i.e., in the almucantar measurements.

However, this is totally different when $\mu \neq \mu_0$, i.e., in the principal plane measurements. Dividing Eq. (27) by Eq. (28), we obtain

$$
\begin{aligned}
\frac{L^{2-\mathrm{lyr}}(\hat{\xi})}{L^{1-\mathrm{lyr}}(\hat{\xi})} &= \frac{\tau_r+\tau_a}{\tau_r} \\
&\times \left\{\frac{[\exp(-\tau_r/\mu_0) - \exp(-\tau_r/\mu)]\exp(-\tau_a/\mu)}{\exp[-(\tau_r+\tau_a)/\mu_0] - \exp[-(\tau_r+\tau_a)/\mu]}\right\}. \qquad (30)
\end{aligned}
$$

When $1/\mu \gg 1/\mu_0$, i.e., the viewing angle is close to 90°, Eq. (30) simplifies to

$$
\frac{L^{2-\mathrm{lyr}}(\hat{\xi})}{L^{1-\mathrm{lyr}}(\hat{\xi})} = \frac{\tau_r+\tau_a}{\tau_r}\,\frac{\exp(-\tau_a/\mu)}{\exp(-\tau_a/\mu_0)}. \qquad (31)
$$

In this case, the radiance calculated with the one-layer model is much larger than the radiance calculated with the two-layer model. Consequently, large errors in the volume scattering function are created at scattering angles corresponding to near-horizon viewing angles (for example, $\theta = 85°$ or $\Theta = 145°$). This, along with multiple scattering, explains the

sharp increase of the error in the volume scattering function from 120° to 145°.

The above retrieval results and analysis demonstrate that very large errors can be incurred by the oversimplified two-layer model in the case of absorbing aerosols. It is necessary to evaluate the effect of aerosol vertical inhomogeneity on retrieval for absorbing aerosols when there is a significant mixture of Rayleigh and aerosol scattering. For a more realistic estimate of the extent of the error caused by aerosol vertical structure, we created the modified two-layer model. In this model, the upper layer contains exclusively Rayleigh scattering molecules, and the lower layer contains thoroughly mixed aerosols and Rayleigh scattering molecules. If we assume the lower layer extends 2 km above the ground, at standard surface pressure, $\tau_r = 0.05073$ at 443 nm and $\tau_r = 0.00334$ at 865 nm in the lower layer. In the upper layer, $\tau_r = 0.18533$ and 0.01220 at 443 and 865 nm, respectively. (The total optical thicknesses for Rayleigh scattering at 443 and 865 nm are, respectively, 0.23606 and 0.01554.) Although a great deal of simplification has been made in this model, it reasonably reflects the mixture of aerosol and Rayleigh scattering.

Figures 8(c) and 8(d) show the retrieval results at 865 and 443 nm, respectively. This modified two-layer model is used to create the pseudodata, and the unmodified two-layer model (all aerosol scattering in the bottom layer and all Rayleigh scattering in the top layer) is used in the retrieval. The conditions assumed in Figs. 8(c) and 8(d) are otherwise identical to the conditions in Figs. 8(a) and 8(b). These results show that at 865 nm there is very little error resulting from the incorrect assumption regarding vertical inhomogeneity. Although the aerosol single-scattering albedo can be retrieved successfully at 443 nm (<1% error), errors in the volume scattering function are significant. For example, the largest error in the volume scattering function is more than 160%, which occurs at $\Theta = 145°$. These results demonstrate that, for the purpose of retrieving the aerosol volume scattering function, when dealing with absorbing aerosols the vertical distribution of aerosols and Rayleigh scattering molecules need to be carefully taken into account, e.g., with lidar measurements.[47] In such cases, the retrieval algorithm can be revised to include the observed vertical structure to ensure successful retrieval.

E. Effects of Errors in the Sky Radiance

We examine two types of error in the sky radiance measurements: random errors and systematic errors. Random errors are due to random noise in the instrument. The random noise is usually considered to have a Gaussian distribution. Systematic errors are due to the uncertainty in the conversion of electronic signals to radiance resulting in calibration uncertainty. They are usually less than 5%. In fact, it is now possible to calibrate a radiometer relative to a standard lamp to within ±2.5%,[48] although

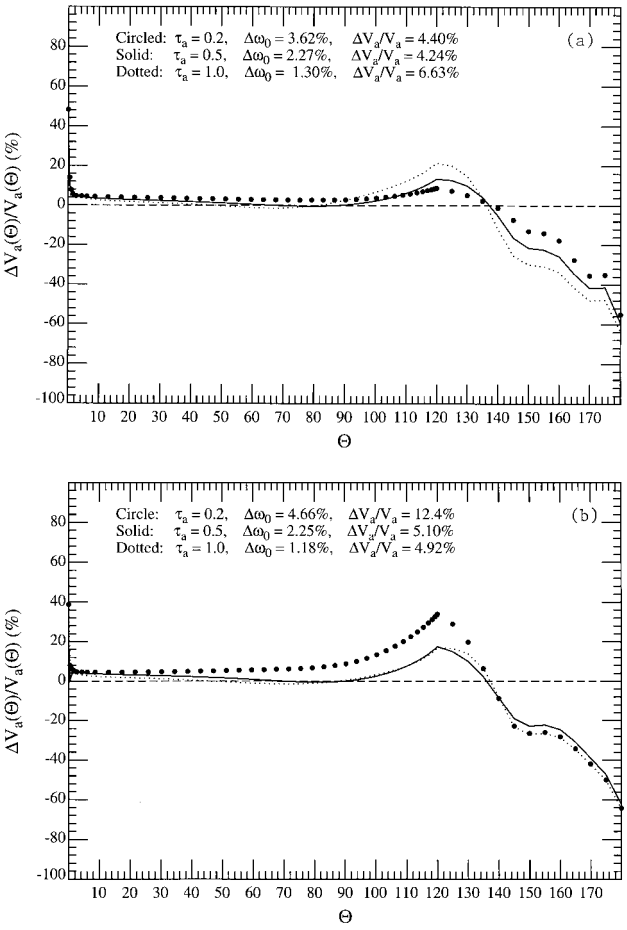

Fig. 9. Retrieved errors when there is a +5% systematic error in the sky radiance: (a) λ = 865 nm and (b) λ = 443 nm.

it is believed that detector-based calibration could reduce the uncertainty to ±1%.[49]

Simulating systematic errors is straightforward. We can simply add a fixed percentage to the true radiance in all viewing directions, i.e.,

$$L^{(m)}(\hat{\xi}_i) = L^{(t)}(\hat{\xi}_i) + \rho_0 L^{(t)}(\hat{\xi}_i), \tag{32}$$

where $L^{(m)}$ is the measured radiance, $L^{(t)}$ is the true radiance, and ρ_0 is the systematic error. Simulating random errors is somewhat more complicated. One needs to create random errors according to the Gaussian distribution and then add them to the sky radiance in different directions.

$$L^{(m)}(\hat{\xi}_i) = L^{(t)}(\hat{\xi}_i) + \rho_i L^{(t)}(\hat{\xi}_i), \tag{33}$$

where

$$P(\rho_i) = \frac{1}{\sqrt{2\pi\sigma^2}} \exp(-\rho_i^2/2\sigma^2), \tag{34}$$

where ρ_i is the noise, $P(\rho_i)$ is the normalized distribution of ρ_i, and σ^2 is the variance of the noise. In the radiance calculation, we assumed a Lambertian surface, the albedo of which is 1.0 at 865 nm and 0.5 at 443 nm.

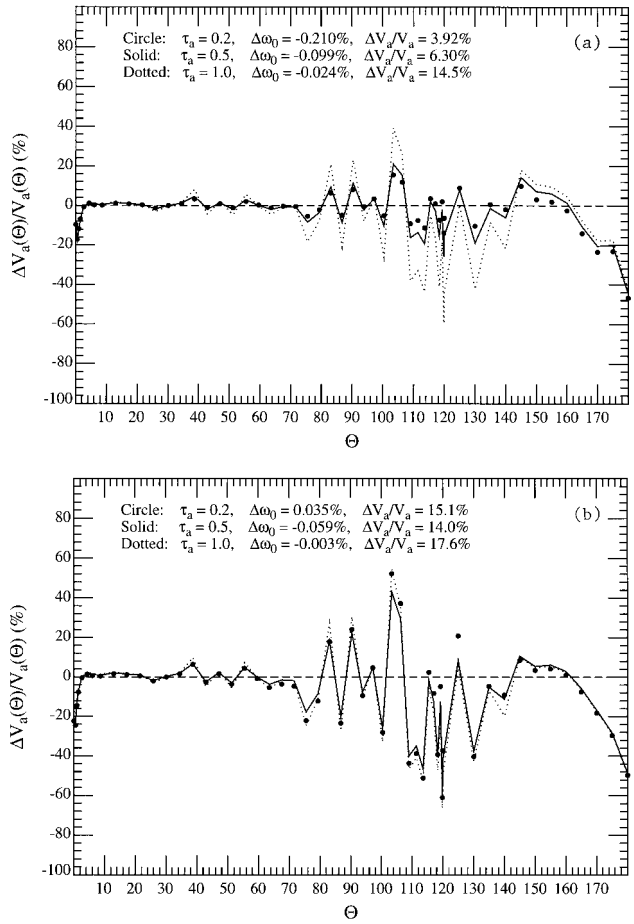

Fig. 10. Retrieval errors when there is a 1% random error in the sky radiance for (a) λ = 865 nm and (b) λ = 443 nm.

1. *Systematic Errors*

Figure 9 shows the retrieval results at 865 and 443 nm for the C80 aerosol when there are +5% systematic errors in the sky radiance, but no random errors. We observed that, in all the curves, errors in the aerosol volume scattering function increase as the scattering angle increases. The retrieval results at 865 nm are acceptable. The largest error in the single-scattering albedo is less than 4%, and the largest average error in the volume scattering function is less than 7%. In comparison, the retrieval results at 443 nm are much worse. At $\tau_a = 0.2$, the error in the single-scattering albedo is 4.66%, and the average error in the volume scattering function is 12.4%. Rayleigh scattering is believed to be largely responsible for the foregoing result. In the single-scattering approach, the sky radiance is given by

$$L^{(t)}(\hat{\xi}) = \frac{\tau_a}{|\hat{\xi}\cdot\hat{n}|} V_a(\hat{\xi}_0 \to \hat{\xi}) + \frac{\tau_r}{|\hat{\xi}\cdot\hat{n}|} V_r(\hat{\xi}_0 \to \hat{\xi}), \quad (35)$$

where τ_r and τ_a are the Rayleigh optical thickness and aerosol optical thickness, respectively; V_a is the aerosol volume scattering function; and V_r is the Rayleigh volume scattering function. Rearranging Eq. (35), one can obtain the aerosol volume scattering function:

$$V_a(\hat{\xi}_0 \to \hat{\xi}) = \frac{L^{(t)}(\hat{\xi})|\hat{\xi}\cdot\hat{n}| - \tau_r V_r(\hat{\xi}_0 \to \hat{\xi})}{\tau_a}. \quad (36)$$

It is easy to prove that, if the systematic error in $L^{(t)}$ is ρ_0, the error in the aerosol volume scattering function $\Delta V_a/V_a$ is

$$\frac{\Delta V_a(\hat{\xi}_0 \to \hat{\xi})}{V_a(\hat{\xi}_0 \to \hat{\xi})} = \rho_0 \frac{\tau_a V_a(\hat{\xi}_0 \to \hat{\xi}) + \tau_r V_r(\hat{\xi}_0 \to \hat{\xi})}{\tau_a V_a(\hat{\xi}_0 \to \hat{\xi})}. \quad (37)$$

It is evident in Eq. (37) that the error in the volume scattering function increases as τ_r increases. Also, the error is larger in the viewing directions where the aerosol volume scattering function is smaller. In other words, errors at large scattering angles are much larger than those at small scattering angles because the aerosol volume scattering function is forwardly peaked and is usually small at large scattering angles.

Our algorithm has been developed assuming that τ_a and L_t are measured by two separate instruments; however, if they are measured with the same instrument, absolute calibration is not necessary. Nakajima *et al.*[16] show how this can be effected by accurately determining the solid angle viewed by the radiometer. Such a procedure would considerably reduce the systematic error below the 5% assumed here.

2. *Random Errors*

Figure 10 shows the retrieval results at 865 and 443 nm, respectively, when there are 1% random errors in the sky radiance, i.e., the noise is Gaussian with a standard deviation of 1%. No systematic error was assumed. The error in the volume scattering function increases as the aerosol optical thickness increases. Errors become extremely large at large scattering angles at 865 nm and even larger at 443 nm. However, errors in the single-scattering albedo are not significant. The largest error in the single-scattering albedo is only −0.21%. This is easily understandable. The single-scattering albedo is simply the integral of the volume scattering function over all solid angles. Because errors in the volume scattering function at different angles have different signs because of the random nature of noise, they offset each other in the integral.

The large errors in the volume scattering functions result from the combined effects of multiple scattering and the surface contribution. Recall that, in the absence of Rayleigh scattering, if we consider only multiple scattering to the second order and the surface contribution to the first order, the sky radiance can be expressed as follows:

$$L_t(\hat{\xi}) = L_{10}(\hat{\xi}) + L_{1s}(\hat{\xi}) + L_{20}(\hat{\xi}), \quad (38)$$

where

$$L_{10}(\hat{\xi}) = F_0 \frac{\tau_a}{|\hat{\xi}\cdot\hat{n}|} V_a(\hat{\xi}_0 \to \hat{\xi}), \tag{39}$$

$$L_{1s}(\hat{\xi}) = F_0\tau_a \frac{\omega_l|\hat{\xi}_0\cdot\hat{n}|}{|\hat{\xi}\cdot\hat{n}|} \int_{\hat{\xi}'\cdot\hat{n}>0} V_a(\hat{\xi}\to\hat{\xi}')\mathrm{d}\Omega(\hat{\xi}'), \tag{40}$$

$$L_{20}(\hat{\xi}) = F_0 \frac{\tau_a^2}{2} \int_{4\pi} \frac{V_a(\hat{\xi}_0\to\hat{\xi}')V_a(\hat{\xi}'\to\hat{\xi})}{|\hat{\xi}'\cdot\hat{n}||\hat{\xi}\cdot\hat{n}|}\,\mathrm{d}\Omega(\hat{\xi}'). \tag{41}$$

In Eqs. (38)–(41), L_{10} is single-scattering radiance in the absence of a surface, L_{1s} is the surface contribution to single-scattering radiance, and L_{20} is the double-scattering contribution to radiance in the absence of a surface.

Suppose the random error in the volume scattering function at a given scattering angle Θ_i is δ_i as a result of the noise in the radiance. The error in the single-scattering radiance is

$$\Delta L_{10}(\hat{\xi}_i) = \delta_i L_{10}(\hat{\xi}_i). \tag{42}$$

Double scattering L_{20} and the surface contribution L_{1s} involve integrals of the volume scattering function. The errors in the volume scattering function offset each other in the integrals. Consequently, little error is incurred in the surface term and the multiple-scattering term. The total error in the radiance is simply the error in L_{s0}.

$$\Delta L_t(\hat{\xi}_i) = \delta_i L_{s0}. \tag{43}$$

If we divide both sides of Eq. (43) by L_t and rearrange it, we obtain

$$\delta_i = \frac{L_t(\hat{\xi}_i)}{L_{10}(\hat{\xi}_i)} \frac{\Delta L_t(\hat{\xi}_i)}{L_t(\hat{\xi}_i)}, \tag{44}$$

where $\Delta L_t(\hat{\xi}_i)/L_t(\hat{\xi}_i)$ is the random error in the radiance, what we call ρ_i. Equation (44) shows that the error in the volume scattering function is the error in the radiance magnified by the ratio of total radiance to the single-scattering radiance. The more insignificant single scattering is, or in other words, the more significant multiple scattering and the surface contribution are in the total radiance, the larger the error in the volume scattering function becomes. At large scattering angles from the Sun to the detector, multiple scattering and the surface contribution constitute the major part of the radiance. Consequently, errors in the volume scattering function are very large.

Equation (44) was derived in the absence of Rayleigh scattering. However, it is not difficult to derive that it is still valid if Rayleigh scattering is included, except L_{10} includes only the aerosol contribution, whereas L_t includes both the aerosol and the Rayleigh contributions. In this case, multiple scattering and the surface contribution become even more significant. Consequently, errors in the volume scattering function become even larger.

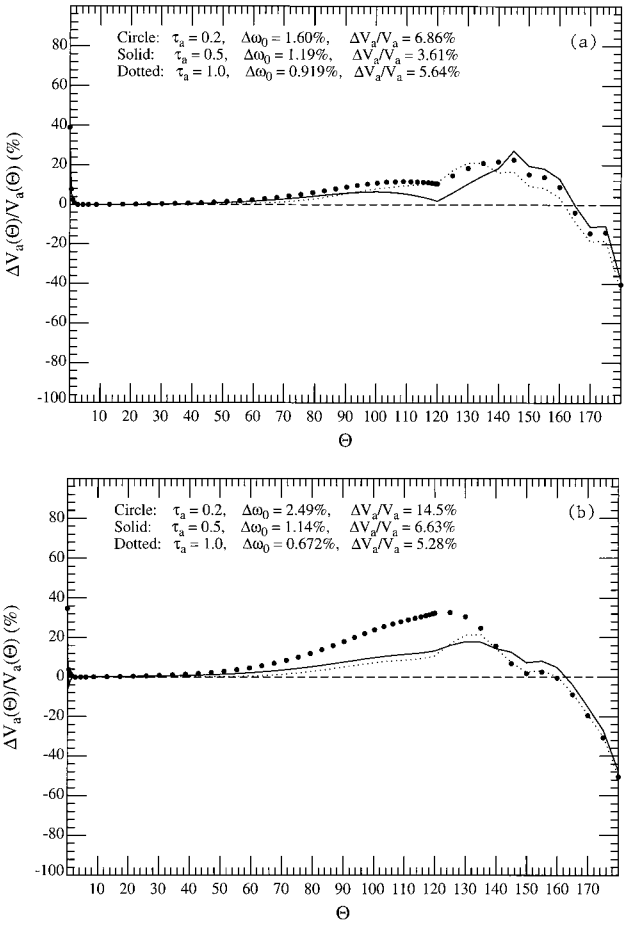

Fig. 11. Retrieval errors when there is a −10% error in the land albedo for (a) λ = 865 nm and (b) λ = 443 nm.

The preceding retrieval results and analysis show that the effect of random errors can be serious. However, in reality, one can successfully reduce them by averaging the retrieved volume scattering function over a range of angles, or by averaging the resulting $V_a(\Theta)$ derived from independent sequential sets of data. Alternatively, if an all-sky camera[50] is used to acquire the sky radiance at all angles simultaneously, independent measurements of the sky radiance could be averaged to reduce noise. Therefore random errors do not present a real threat to retrieval.

F. Effect of Errors in Land Albedo

For a land surface with a BRDF that varies over a large range, it is difficult to measure the surface albedo with high accuracy. Even for a land surface that is close to Lambertian, significant errors can still be incurred in actual measurements of the surface albedo. Figure 11 shows the retrieval results at 865 and 443 nm for the C80 aerosol when incorrect surface albedos are used. The true land albedos are 1.0 at 865 nm and 0.5 at 443 nm. The albedos of 0.9 at 865 nm and 0.45 at 443 nm were used in the retrieval. A Lambertian surface was assumed in all simulations.

The retrieval results at 865 nm are acceptable. The largest errors in the single-scattering albedo (1.60%) and volume scattering function (6.86%) both occur at the optical thickness of 0.2. They decrease as the aerosol optical thickness increases. The results at 443 nm demonstrate the same trend. However, they are significantly poorer than the results at 865 nm. The largest error in the aerosol volume scattering function and the single-scattering albedo are 14.5% and 2.49% respectively, which occur at $\tau_a = 0.2$.

These results can be explained as follows. Rayleigh scattering dominates backscattering. A thick Rayleigh layer at 443 nm increases backscattering, thereby increasing the surface contribution to sky radiance. These errors induced by the biased land albedo are much larger at 443 nm than those at 865 nm. Because all the errors resulting from the biased land albedos are allocated to the aerosol volume scattering function, errors in the aerosol volume scattering function and consequently the error in the single-scattering albedo are much larger at 443 nm than those at 865 nm. At a given wavelength, as the aerosol optical thickness increases, the error in the surface contribution does not increase significantly because the major part of the surface contribution comes from Rayleigh scattering. The implication therefore is that the errors become less significant in relation to the radiance caused by aerosol scattering. Consequently, the error in the aerosol volume scattering function and the single-scattering albedo decreases as the aerosol optical thickness increases. It is important to note that these results were derived for situations with an unrealistically high surface albedo so as to maximize the error. In reality, the effect of a 10% error in surface albedo would be less than these simulations suggest because the contribution resulting from surface interactions would be less.

5. Conclusion

In this paper we illustrated a scheme that applies recursive procedures to retrieve columnar properties of aerosols, i.e., the scattering phase function and single-scattering albedo, from the sky radiance.

When measurements are performed under ideal conditions, i.e., actual conditions are in total agreement with the approximations made in the retrieval algorithm, the overall retrieval results are excellent. The error in the single-scattering albedo is usually within a fraction of 1%. The average error in the volume scattering function is usually well within 3%. However, we did find that, because of the inability to measure the sky radiance in directions close to the direct solar beam, relatively large errors in the retrieved aerosol volume scattering function occurred in the blue when the true aerosol phase function was extremely sharp (U99).

Subsequent studies concentrated on the susceptibility of the retrieval algorithm to measurement errors and conditions deviating from the approximations made in the retrieval algorithm. These conditions include non-Lambertian reflectance of a land surface (the BRDF effect); surface inhomogeneity, as well as horizontal aerosol inhomogeneity; and incorrect aerosol vertical structure. These studies reveal that the retrieval algorithm places certain restrictions on the land BRDF. When the land deviates significantly from the Lambertian approximation, e.g., the irrigated wheat surface, significant errors are found in the single-scattering albedo and, particularly, in the volume scattering function. Error that is due to an incorrect vertical structure for the aerosol is significant only when the aerosol is strongly absorbing. This source of error could be virtually eliminated with use of simultaneous lidar observations to infer the coarse vertical structure of the aerosol.

Table 2. Summary of the Error in ω_0 at 865 nm

Situation	$\Delta\omega_0$ (%)
Ideal Case	<0.2
Non-Lambertian: stepped grass ($\omega_l = 0.29$, $\tau_a = 0.2$)	<0.4
Non-Lambertian: irrigated wheat ($\omega_l = 0.58$, $\tau_a = 0.2$)	<2.5
Horizontal surface inhomogeneity ($\omega_l = 0.4$, $\tau_a = 0.2$)	<0.3
Horizontal aerosol inhomogeneity ($\omega_l = 1.0$, $\tau_a = 0.2$)	<0.8
Incorrect vertical structure ($\omega_l = 1.0$, $\tau_a = 1.0$, U00)	<1.4
5% error in L_t ($\omega_l = 1.0$, $\tau_a = 0.2$)	<3.7
1% random error in L_t ($\omega_l = 1.0$, $\tau_a = 0.2$)	<0.3
5% error in ω_l ($\omega_l = 1.0$, $\tau_a = 0.2$)	<1.6

These studies also reveal that a certain degree of horizontal aerosol homogeneity is required at 865 nm to ensure accurate retrieval. To achieve the same accuracy at 443 nm, the aerosol must be horizontally homogeneous over approximately twice the distance required at 865 nm. The effects of measurement errors in surface albedo, as well as in the sky radiance on the retrieval results, have also been discussed. Aside from the error in surface albedo and BRDF, the most serious effect is from the systematic error in sky radiance. Serious error would result from this when the aerosol optical thickness is low and, simultaneously, when the Rayleigh optical thickness is high. However, use of the calibration technique of Nakajima *et al.*[16] should significantly reduce such systematic errors in the measurements.

Table 2 summarizes the error in ω_0 at 865 nm under various conditions. Even when actual conditions deviate significantly from the approximations made in the retrieval program, the error in the single-scattering albedo is usually small. This suggests that the retrieval algorithm, without any further adjustment, can be successfully applied quantitatively to identify the presence of strongly absorbing aerosols. The retrieval results for the phase function are not quite as good as for ω_0. Generally, the errors are small at small scattering angles, but they can become quite large for large scattering angles. However, in most of our calculations, the average errors in the volume scattering function are less than 5% at 865 nm and less than 10% at 443 nm.

Overall, the retrieval results at 443 nm, with the exception of the BRDF effect, are much less satisfactory than those at 865 nm. At 443 nm, the retrieval

results are more susceptible to land heterogeneity, vertical and horizontal aerosol inhomogeneity, systematic error in the sky radiance, etc., especially for low aerosol optical thickness. Simulations show that, when there is large systematic (calibration) error in the sky radiance measurements, or when the land is strongly inhomogeneous on large (~1 km) scales, the error in the single-scattering albedo can be as large as 10% or even higher at very low aerosol optical thickness ($\leq$0.05). Error in the aerosol volume scattering function can be as large as 40%.

Although in the present retrieval algorithm we used scalar radiative transfer theory (ignoring polarization), we believe that similar results could be obtained with vector theory. Gordon and Zhang[20] studied the accuracy with which the TOA radiance over water could be derived from a phase function and ω_0 deduced from sky radiance using a retrieval algorithm similar to that presented here. For their study, it was found that ignoring polarization was important in the TOA radiance, i.e., the errors in the TOA radiance, resulting from the errors in the scattering phase function at large scattering angles, were typically small ($\leq$2.5%). (Later, Zhang and Gordon[23,24] developed an inversion algorithm that included polarization, enabling derivation of the 11 and 12 elements of the scattering phase matrix and leading to improvements in the predicted TOA radiance.) Unlike the ocean, which polarizes the light field on reflection, the land will normally depolarize it; therefore we expect the effects of polarization on this algorithm over land to be significantly less severe than over the oceans.

On the basis of our computations, it is clear that this algorithm works best when both τ_r and ω_l are small. This suggests that the best wavelength for its application would be near 670 nm, i.e., near the short-wave edge of the high-reflectance region for vegetated surfaces.

We believe that this algorithm, combined with the Nakajima *et al*.[16] algorithm could be used to provide information regarding aerosol nonsphericity in the following way. In most cases, our algorithm provides excellent retrievals of the phase function for $\Theta \lesssim 90°$. Computations[18] show that significant effects of nonsphericity are seen in the phase function for $\Theta \gtrsim 30°$. Thus comparison of the Mie-based phase functions derived by the Nakajima *et al*. inversion algorithm, with the phase function based on our inversion in the range $30° \lesssim \Theta \lesssim 90°$, may provide particle shape information.

In this study we have sought to delineate the magnitudes of the error inherent in this method when the assumptions made in the algorithm are incorrect. To demonstrate the effects, in many cases our assignment of values for the parameters have been extreme, e.g., $\omega_l = 1$. Thus we recommend that anyone using this algorithm perform a detailed sensitivity analysis specific to the characteristics of their actual measurement site.

The authors gratefully acknowledge the National Aeronautics and Space Administration for support under grant NAGW-273 and contracts NAS5-31363 and NAS5-31734. The authors are also grateful to an anonymous reviewer for pointing out the relationship between the Wang and Gordon algorithm and the Newton–Raphson method and for making several suggestions that significantly improved the paper.

References

1. R. J. Charlson, J. E. Lovelock, M. O. Andreae, and S. G. Warren, "Oceanic phytoplankton, atmospheric sulphur, cloud albedo and climate," Nature (London) **326,** 655–661 (1987).
2. R. J. Charlson, S. E. Schwartz, J. M. Hales, R. D. Cess, J. A. Coakley, J. E. Hansen, and D. J. Hofmann, "Climate forcing by anthropogenic aerosols," Science **255,** 423–430 (1992).
3. Y. J. Kaufman, "Remote sensing of direct and indirect aerosol forcing," in *Aerosol Forcing of Climate*, R. H. Charlson and J. Heintzenberg, eds. (Wiley, New York, 1995), pp. 297–332.
4. V. V. Salomonson, W. L. Barnes, P. W. Maymon, H. E. Montgomery, and H. Ostrow, "MODIS: advanced facility instrument for studies of the Earth as a system," IEEE Trans. Geosci. Remote Sensing **27,** 145–152 (1989).
5. D. J. Diner, C. J. Bruegge, J. V. Martonchik, T. P. Ackerman, R. Davies, S. A. W. Gerstl, H. R. Gordon, P. J. Sellers, J. Clark, J. A. Daniels, E. D. Danielson, V. G. Duval, K. P. Klaasen, G. W. L. A. D. I. Nakamoto, R. Pagano, and T. H. Reilly, "MISR: a multi-angle imaging spectroradiometer for geophysical and climatological research from EOS," IEEE Trans. Geosci. Remote Sensing **27,** 200–214 (1989).
6. P. Y. Deschamps, F. M. Bréon, M. Leroy, A. Podaire, A. Bricaud, J. C. Buriez, and G. Sèze, "The POLDER mission: instrument characteristics and scientific objectives," IEEE Trans. Geosci. Remote Sensing **32,** 598–615 (1994).
7. M. Wang and H. R. Gordon, "Estimating aerosol optical properties over the oceans with the multiangle imaging spectroradiometer: some preliminary studies," Appl. Opt. **33,** 4042–4057 (1994).
8. M. Wang and H. R. Gordon, "Estimation of aerosol columnar size distribution and optical thickness from the angular distribution of radiance exiting the atmosphere: simulations," Appl. Opt. **34,** 6989–7001 (1995).
9. W. A. Hoppel, J. W. Fitzgerald, G. M. Frick, R. E. Larson, and E. J. Mack, "Aerosol size distributions and optical properties found in the marine boundary layer over the Atlantic Ocean," J. Geophys. Res. **95D,** 3659–3686 (1990).
10. E. P. Shettle and R. W. Fenn, "Models for the aerosols of the lower atmosphere and the effects of humidity variations on their optical properties," AFGL-TR-79-0214 (Air Force Geophysics Laboratory, Hanscomb Air Force Base, Mass., 1979).
11. G. A. d'Almeida, P. Koepke, and E. P. Shettle, *Atmospheric Aerosols—Global Climatology and Radiative Characteristics* (A. Deepak, Hampton, Va., 1991).
12. H. R. Gordon and M. Wang, "Retrieval of water-leaving radiance and aerosol optical thickness over the oceans with SeaWiFS: a preliminary algorithm," Appl. Opt. **33,** 443–452 (1994).
13. H. R. Gordon, "Atmospheric correction of ocean color imagery in the Earth observing system era," J. Geophys. Res. **102D,** 17081–17106 (1997).
14. B. N. Holben, T. F. Eck, I. Slutsker, D. Tanre, J. P. Buis, A. Setzer, E. Vermote, J. A. Reagan, Y. J. Kaufman, T. Nakajima, and F. Lavenu, "Multi-band automatic Sun and sky scanning radiometer system for measurement of aerosols," presented at the Sixth International Symposium on Physical Measurements and Signatures in Remote Sensing, Val-d'Isère, France, 17–21 January 1994.

15. T. Nakajima, M. Tanaka, and T. Yamauchi, "Retrieval of the optical properties of aerosols from aureole and extinction data," Appl. Opt. **22,** 2951–2959 (1983).
16. T. Nakajima, G. Tonna, R. Rao, P. Boi, Y. Kaufman, and B. Holben, "Use of sky brightness measurements from ground for remote sensing of particulate polydispersions," Appl. Opt. **35,** 2672–2686 (1996).
17. Y. J. Kaufman, A. Gitelson, A. Karnieli, E. Ganor, R. S. Eraser, T. Nakajima, S. Mattoo, and B. N. Holben, "Size distribution and scattering phase functions of aerosol particles retrieved from sky brightness measurements," J. Geophys. Res. **99D,** 10341–10356 (1994).
18. M. I. Mishchenko and L. D. Travis, "Light scattering by polydispersions of randomly oriented spheriods with sizes comparable to wavelengths of observation," Appl. Opt. **33,** 7206–7225 (1994).
19. M. Wang and H. R. Gordon, "Retrieval of the columnar aerosol phase function and single scattering albedo from sky radiance over the ocean: simulations," Appl. Opt. **32,** 4598–4609 (1993).
20. H. R. Gordon and T. Zhang, "How well can radiance reflected from the ocean–atmosphere system be predicted from measurements at the sea surface?," Appl. Opt. **35,** 6527–6543 (1996).
21. H. R. Gordon and T. Zhang, "Columnar aerosol properties over oceans by combining surface and aircraft measurements: simulations," Appl. Opt. **34,** 5552–5555 (1995).
22. T. Zhang and H. R. Gordon, "Columnar aerosol properties over oceans by combining surface and aircraft measurements: sensitivity analysis," Appl. Opt. **36,** 2650–2662 (1997).
23. T. Zhang and H. R. Gordon, "Passive remote sensing of elements of the aerosol scattering matrix: simulations," in *Optical Remote Sensing of the Atmosphere*, Vol. 5 of 1997 OSA Technical Digest Series (Optical Society of America, Washington, D.C., 1997), pp. 158–160.
24. T. Zhang and H. R. Gordon, "Retrieval of elements of the columnar aerosol scattering phase matrix from polarized sky radiance over the ocean: simulations," Appl. Opt. **36,** 7948–7959 (1997).
25. M. Wendisch and W. von Hoyningen-Huene, "High speed version of the method of 'successive order of scattering' and its application to remote sensing," Beitr. Phys. Atmos. **64,** 83–91 (1991).
26. N. J. McCormick, "Inverse radiative transfer problems: a review," Nucl. Sci. Eng. **112,** 185–198 (1992).
27. T. Nakajima and M. Tanaka, "Effect of wind-generated waves on the transfer of solar radiation in the atmosphere-ocean system," J. Quant. Spectrosc. Radiat. Transfer **29,** 521–537 (1983).
28. C. Cox and W. Munk, "Measurements of the roughness of the sea surface from photographs of the Sun's glitter," J. Opt. Soc. Am. **44,** 838–850 (1954).
29. H. R. Gordon and M. Wang, "Influence of oceanic whitecaps on atmospheric correction of SeaWiFS," Appl. Opt. **33,** 7754–7763 (1994).
30. J. E. Hansen and L. D. Travis, "Light scattering in planetary atmospheres," Space Sci. Rev. **16,** 527–610 (1974).
31. F. X. Kenizys, E. P. Shettle, W. O. Gallery, J. H. Chetwynd, L. W. Abreu, J. E. A. Selby, S. A. Clough, and R. W. Fenn, "Atmospheric Transmittance/Radiance: The LOWTRAN 6 Model," AFGL-TR-83-0187 (Air Force Geophysics Laboratory, Hanscomb Air Force Base, Mass., 1983).
32. K. P. Bowman and A. J. Krueger, "A global climatology of total ozone from the nimbus 7 total ozone mapping spectrometer," J. Geophys. Res. **90D,** 7967–7976 (1985).
33. M. D. King and D. M. Byrne, "A method for inferring total ozone content from the spectral variation of optical depth obtained with a solar radiometer," J. Atmos. Sci. **35,** 2242–2251 (1976).
34. R. W. Preisendorfer and C. D. Mobley, "Direct and inverse irradiance models in hydrologic optics," Limnol. Oceanogr. **29,** 903–929 (1984).
35. H. R. Gordon and D. J. Castaño, "Aerosol analysis with the coastal zone color scanner: a simple method for including multiple scattering effects," Appl. Opt. **28,** 1320–1326 (1989).
36. H. C. van de Hulst, *Multiple Light Scattering* (Academic, New York, 1980).
37. P. Y. Deschamps, M. Herman, and D. Tanre, "Modeling of the atmospheric effects and its application to the remote sensing of ocean color," Appl. Opt. **22,** 3751–3758 (1983).
38. W. H. Press, B. P. Flannery, S. A. Teukolsky, and W. T. Vetterling, *Numerical Recipes in FORTRAN* (Cambridge U. Press, Cambridge, England, 1992).
39. D. T. Lindgren, "Land use planning and remote sensing," in *Remote Sensing of Earth Resources and Environment* (Dordrecht, Boston, Mass., 1985), p. 176.
40. C. Elachi, Introduction to the Physics and Techniques of Remote Sensing (Wiley, New York, 1987), p. 413.
41. M. D. King and B. M. Herman, "Determination of the ground albedo and the index of absorption of atmospheric particulates by remote sensing. Part I: Theory," J. Atmos. Sci. **36,** 163–173 (1979).
42. D. S. Kimes, "Dynamics of directional reflectance factor distributions for vegetation canopies," Appl. Opt. **22,** 1364–1372 (1983).
43. D. S. Kimes, W. W. Newcomb, and C. J. Tucker, "Directional reflectance factor distributions for cover types of Northern Africa," Remote Sensing Environ. **18,** 1–19 (1985).
44. J. A. Kirchner, D. S. Kimes, and J. E. McMurtrey III, "Variation of directional reflectance factors with structural changes of a developing alfalfa canopy," Appl. Opt. **21,** 3766–3774 (1982).
45. D. S. Kimes, W. W. Newcomb, R. F. Nelson, and J. B. Schutt, "Directional reflectance factor distributions of a hardwood and pine forest canopy," IEEE Trans. Geosci. Remote Sensing **24,** 281–293 (1986).
46. T. Zhang, "Remote sensing of aerosol properties over the ocean by combining surface and aircraft measurements," Ph.D. dissertation (University of Miami, Coral Gables, Fla., 1995).
47. Y. Sasano and E. V. Browell, "Light scattering characteristics of various aerosol types derived from multiple wavelength lidar observations," Appl. Opt. **28,** 1670–1679 (1989).
48. S. F. Biggar, P. N. Slater, and D. I. Gellman, "Uncertainties in the in-flight calibration of sensors with reference to measured ground sites in the 0.4 to 1.1 μm range," Remote Sensing Environ. **48,** 245–252 (1994).
49. P. N. Slater, S. F. Biggar, K. J. Thome, D. I. Gellman, and P. R. Spyak, "Vicarious radiometric calibration of EOS sensors," J. Atmos. Oceanic Technol. **13,** 349–359 (1996).
50. K. J. Voss and G. Zibordi, "Radiometric and geometric calibration of a visible spectral electro-optic 'Fisheye' camera radiance distribution system," J. Atmos. Oceanic Technol. **6,** 652–662 (1989).